Macromolecular Materials and Engineering

Macromolecular Materials and Engineering Open Access

www.mame-journal.de

RESEARCH ARTICLE OPEN ACCESS

Sustainable Bioactive Hydrogels Engineered with *Liquidambar orientalis* Extracts: pH-Dependent Release Behavior and Wound Healing Potential

Meltem Taş Küçükaydın[1] | Mehmet Emin Duru[1] | Aydın Demiray[2] | Selçuk Küçükaydın[3] | Özgür Ceylan[4]

[1]Department of Chemistry, Faculty of Science, Muğla Sıtkı Koçman University, Muğla, Turkey | [2]Department of Medical Genetics, Faculty of Medicine, Pamukkale University, Denizli, Turkey | [3]Department of Medical Services and Techniques, Köyceğiz Vocational School of Health Services, Muğla Sıtkı Koçman University, Köyceğiz/Muğla, Turkey | [4]Food Quality Control and Analysis Program, Ula Ali Kocman Vocational School, Muğla Sıtkı Koçman University, Ula/Mugla, Turkey

Correspondence: Selçuk Küçükaydın (selcukkucukaydin@mu.edu.tr)

Received: 12 February 2026 | **Revised:** 26 May 2026 | **Accepted:** 4 June 2026

Keywords: bioactive materials | chitosan | hydrogel films | liquidambar orientalis | pH-dependent release | wound dressing

ABSTRACT

Bioactive hydrogel films were developed by incorporating *Liquidambar orientalis* leaf extract (LOLE) and resin extract (LORE) into PVA/starch, PVA/chitosan, chitosan/gelatin, and chitosan matrices. HPLC-DAD identified myricetin as a major LOLE marker and trans-cinnamic acid as the predominant LORE compound, while SEM and FT-IR analyses supported extract incorporation and possible interactions within the hydrogel networks. The films exhibited polymer- and extract-dependent physicochemical behavior. LOLE-loaded chitosan films showed the highest swelling capacity (350%) and the highest in vitro mass loss after 14 days. Release studies demonstrated matrix-dependent and pH-dependent behavior within the tested pH range, with faster release generally observed at pH 5.5 than at pH 7.4; LOLE-loaded chitosan/gelatin films released 85.3% of the extract within 12 h at pH 5.5. LOLE-loaded hydrogels showed stronger antioxidant activity, whereas LORE-loaded films exhibited stronger antimicrobial performance against wound-associated microorganisms, reflecting their distinct phytochemical profiles. The extracts also showed antibiofilm, anti-quorum sensing, enzyme-inhibitory, and preliminary scratch wound closure activities, with no apparent cytotoxicity toward HEK-293T cells. LORE showed notable tyrosinase inhibition (IC_{50}: 20.18 µg/mL), suggesting pigmentation-related relevance. Overall, these findings support further investigation of *L. orientalis*-derived hydrogel films as sustainable bioactive wound dressing platforms, although mechanical, stability, and in vivo validations remain necessary.

1 | Introduction

Wounds are among the most important health problems affecting humanity worldwide [1]. For centuries, people have used various herbal agents to accelerate wound healing [2]. Plants provide a wide range of therapeutic benefits due to their bioactive constituents, including flavonoids, fatty acids, alkaloids, and carbohydrates. These compounds promote wound healing through diverse mechanisms such as skin tissue regeneration, antioxidant, anti-inflammatory, and antimicrobial activities [3–5]. Wound healing is a complex and dynamic process, and effective materials are required to improve and accelerate it. Traditional wound dressings such as gauze, paraffin gauze, and similar materials have long been used in wound and burn care [6]. However, due to their limitations, new wound dressings have been developed. Modern wound dressings such as hydrogels, films, sprays, and foams, generally prepared from natural and synthetic polymers, are now widely preferred. Their desirable

This is an open access article under the terms of the Creative Commons Attribution License, which permits use, distribution and reproduction in any medium, provided the original work is properly cited.

© 2026 The Author(s). *Macromolecular Materials and Engineering* published by Wiley-VCH GmbH

properties include improved mechanical strength, antimicrobial activity, high fluid absorption capacity, the ability to maintain a moist environment, biodegradability, biocompatibility, and non-toxicity [7–9].

Among these, hydrogel dressings stand out because of their similarity to body tissues, high compatibility with living cells, and ability to retain moisture at the wound surface. These characteristics make them ideal candidates for wound management [10]. Recently, increasing attention has been given to incorporating natural products containing bioactive compounds into hydrogel dressings, aiming to enhance their therapeutic potential [11–13].

Liquidambar orientalis Mill. an endemic tree species distributed along the southwestern coastal region of Turkey and commonly known as Sweetgum or Sığla/Günlük tree, has been widely used in phytotherapy due to its medicinal and cosmetic properties [12, 14, 15]. Sweetgum resin has been valued since antiquity: the ancient Egyptians used it for embalming, while Cleopatra reportedly employed it as a beauty tonic [16, 17]. In traditional medicine, sweetgum resin has been applied to treat lip cracks, wounds, burns, skin and gastric diseases, and has also been used as a parasiticide and expectorant [14, 18]. Pharmacological studies have further confirmed the diverse biological activities of *L. orientalis* extracts from both resin and leaves, including antimicrobial, antioxidant, anti-ulcerogenic, sedative, anticonvulsant, antipathogenic, and antimutagenic properties [18–22].

Although *Liquidambar orientalis* resin/storax has been investigated in several wound-related or biomaterial studies, the existing literature has predominantly focused on resin-based formulations [12, 13, 23, 24]. In contrast, the contribution of *L. orientalis* leaves, despite their phenolic- and flavonoid-rich composition, remains comparatively underexplored in hydrogel-based wound dressing systems. Moreover, previous studies have generally been limited to single extract types, individual polymeric systems, or selected biological endpoints, leaving the comparative effects of leaf and resin extracts across different hydrogel matrices insufficiently clarified. In particular, how the distinct phytochemical profiles of *L. orientalis* leaf extract (LOLE) and resin extract (LORE) influence the interrelated physicochemical behavior, pH-dependent release, and biological performance of hydrogel dressings has not been systematically addressed. This gap limits the rational selection of both extract type and polymer matrix for the development of bioactive wound dressing platforms.

The polymeric matrices used in this study were selected to provide complementary properties required for wound dressing applications. Poly(vinyl alcohol) (PVA) was chosen because of its good film-forming ability, hydrophilicity, flexibility, and ability to form stable hydrogel networks [25]. Starch was incorporated as a biodegradable, abundant, and hydrophilic polysaccharide that can enhance water uptake and contribute to sustainable material design [26]. Chitosan was selected due to its biodegradability, biocompatibility, hemostatic character, cationic nature, and intrinsic antimicrobial potential, which make it highly relevant for wound dressing systems [27]. Gelatin was included as a protein-based biopolymer with favorable cell-interactive properties and the ability to improve matrix hydration and biological compatibility [28]. Therefore, the use of PVA/starch, PVA/chitosan, chitosan/gelatin, and chitosan matrices allowed us to compare hydrogel systems with different synthetic–natural, polysaccharide-based, and protein–polysaccharide characteristics and to evaluate how polymer composition affects swelling, degradation, extract release, and biological performance.

Therefore, the present study was designed to develop and comparatively evaluate *L. orientalis* leaf extract (LOLE)- and resin extract (LORE)-loaded hydrogel films based on four different polymeric matrices: PVA/starch, PVA/chitosan, chitosan/gelatin, and chitosan. The novelty of this work lies in the combined use of both leaf and resin extracts, rather than focusing solely on resin/storax, and in the systematic comparison of their behavior within multiple hydrogel networks. Specifically, this study aimed to (i) characterize the phenolic profiles of LOLE and LORE by HPLC-DAD, (ii) evaluate the antioxidant, antimicrobial, antibiofilm, anti-quorum sensing, enzyme inhibitory, cytotoxicity, and scratch wound closure activities of the extracts, (iii) investigate the effects of extract type and polymer composition on hydrogel morphology, swelling, degradation, and pH-dependent release behavior, and (iv) evaluate the biological performance of the developed systems. By integrating chemical, physicochemical, release, and biological data, this work seeks to establish structure–composition–function relationships that may guide the rational design of *L. orientalis*-based hydrogel wound dressing materials.

2 | Experimental Section

2.1 | Chemicals and Reagents

PVA (, Mw: 30 000–70 000 g/mol, 87%–90% hydrolyzed), Chitosan (medium molecular weight, degree of deacetylation: >75%), Gelatin (Type B, from bovine skin, bloom strength: ~225 g, Starch (from potato), Glutaraldehyde (25% aqueous solution), Glycerol (99.5%), Acetic acid (glacial), Hydrochloric acid (37%), and Ethanol (absolute, analytical grade) used for hydrogel preparation and extraction, standard phenolic compounds for HPLC analysis (gallic acid, myricetin, trans-cinnamic acid, quercetin, etc.), reagents for antioxidant assays (DPPH, ABTS, β-carotene, copper (II) chloride, BHA, α-tocopherol, etc.), urease from jack bean (type-III, EC 3.5.1.5), tyrosinase from mushroom (EC 1.14.18.1), reagents for cell culture and biological activity tests, including 3-(4,5-Dimethylthiazol-2-yl)-2,5-Diphenyltetrazolium Bromide (MTT), Dulbecco's Modified Eagle Medium (DMEM), and Fetal Bovine Serum (FBS) were purchased from Sigma–Aldrich, (St. Louis, MO, USA) and Merck (Darmstadt, Germany).

2.2 | Plant Material

Samples of *L. orientalis* leaves and resin were obtained from forested areas in the Muğla region (Marmaris–Köyceğiz) during the period from July to September 2021. The collected leaves were shade-dried, ground into fine powder using a mechanical mill, and stored together with the resin at +4°C until use.

2.3 | Extraction

The resin and leaves of *L. orientalis* were subjected to ethanol extraction under ambient conditions for 24 h, repeated five times. Following filtration, the solvent fractions were concentrated under reduced pressure using a rotary evaporator, and the resulting aqueous phase was subsequently dried by freeze-drying.

2.4 | Total Phenolic and Total Flavonoid Contents

The phenolic content of the extracts was quantified as milligrams of pyrocatechol equivalents (PEs) using the Folin–Ciocalteu method [29]. The concentration of total phenolics was calculated using the calibration curve of pyrocatechol with the following regression equation:

$$\text{Absorbance}: 0.0089\ [\text{pyrocatechol}\,(\text{mg})] + 0.0644\ \left(R^2:\ 0.9922\right)$$

Similarly, the flavonoid content of the extracts was expressed in milligrams of quercetin equivalents and measured according to the aluminium nitrate colorimetric method [30]. The total flavonoids were determined from the quercetin calibration curve, using the equation:

$$\text{Absorbance} = 0.0117\,[\text{quercetin}\ (\text{mg})] + 0.0225\ \left(R^2:\ 09960\right)$$

Measurements were performed in triplicate.

2.5 | Analysis of Phenolic Composition

The phenolic profile of LORE and LOLE was analyzed using an HPLC-DAD system [31]. The extracts were dissolved in an 80:20 (v/v) water–methanol mixture and filtered through a 0.20 µm LC membrane filter before injection. Separation was performed on an Inertsil ODS-3 reverse-phase C_{18} column, and detection was carried out at 280 nm using a photodiode array (PDA) detector.

Phenolic constituents were identified by comparing retention times and UV spectra with those of authentic standards. Calibration curves were established through injections of standard phenolics at varying concentrations, enabling both qualitative and quantitative evaluation. The results were reported as milligrams per gram of dry weight (mg/g dw).

2.6 | Determination of Antioxidant Activity

The antioxidant properties of LORE and LOLE were evaluated using β-carotene–linoleic acid, DPPH, ABTS, ferrous ion-chelation, and CUPRAC assays, with BHA, α-tocopherol, and EDTA as standards [32]. Results were expressed as IC_{50} values (µg/mL) and $A_{0.50}$ for the CUPRAC method.

For hydrogel films incorporating the extracts, antioxidant activity was determined via the DPPH radical scavenging method. Square pieces of film (2 × 2 cm) were immersed in 20 mL ethanol. From the resulting solution, 50 µL was mixed with 150 µL DPPH solution and incubated at room temperature in the dark for 30 min. Absorbance was then recorded at 517 nm using a microplate reader [33]. Film-based antioxidant activity was evaluated using standardized film pieces as described in Section 2.17. All antioxidant assays were performed in triplicate.

2.7 | Determination of Antimicrobial Activity

The antimicrobial potential of LOLE and LORE was evaluated against a panel of microorganisms including *Pseudomonas aeruginosa* ATCC 27853, *Bacillus subtilis* ATCC 6633, *Escherichia coli* ATCC 25922, *Staphylococcus aureus* ATCC 25923, *Candida albicans* ATCC 10239, and *Enterobacter aerogenes* ATCC 13048. Bacterial strains were cultured in Nutrient Broth, whereas *C. albicans* was grown in Sabouraud Dextrose Broth. Microtiter plates inoculated with *C. albicans* were incubated at 30°C, while plates with *S. aureus*, *B. subtilis*, and *P. aeruginosa* were incubated at 37°C. Absorbance was recorded at 550 nm, and the minimum inhibitory concentration (MIC) values were determined by the microdilution method [34].

For hydrogel films incorporating the extracts, antimicrobial tests were conducted against *E. coli*, *S. aureus*, and *C. albicans*. Film pieces were cut and tested based on the MIC values previously established for the extracts [35]. Film-based antimicrobial activity was evaluated using standardized film pieces as described in Section 2.17. All antimicrobial assays were performed in triplicate.

2.8 | Biofilm Inhibition

The ability of LOLE and LORE to inhibit biofilm formation was assessed against the same microbial strains used in the antimicrobial assays. Tests were performed at MIC, ½ MIC, ¼ MIC, and ⅛ MIC concentrations, applying the microplate biofilm protocol [36]. Overnight cultures of microorganisms were diluted in tryptose soy broth (TSB) supplemented with 0.25% glucose. A 200 µL aliquot of inoculum was transferred into sterile 96-well plates, and extracts were added at the corresponding concentrations. Plates were incubated statically at 37°C for 48 h. Following incubation, planktonic cells were discarded, and wells were washed with sterile distilled water. Biofilms adhering to the wells were stained with 0.1% (w/v) crystal violet for 10 min at room temperature. After rinsing to remove excess dye, the retained stain was solubilized using 33% (v/v) glacial acetic acid. Biofilm biomass was quantified by measuring absorbance at 550 nm with a spectrophotometer. The assay was performed in triplicate.

2.9 | Anti-Quorum Sensing Activity

To evaluate the quorum-sensing (QS) inhibitory effects of the extracts, three complementary assays were performed: assessment of the QS inhibition mechanism using *Chromobacterium violaceum* CV026, violacein production inhibition assay using *C. violaceum* CV12472, and swarming and swimming motility inhibition assay using *Pseudomonas aeruginosa* PAO1, as previously described in the literature [37]. *Chromobacterium* strains were cultured at 30°C, whereas the *P. aeruginosa* PAO1 strain was cultured at 37°C on Luria–Bertani (LB) agar. For *C. violaceum* CV026, LB medium was supplemented with kanamycin

(10 μg/mL). MIC values of the extracts against the biosensor strains were determined using the broth microdilution method. Anti-QS activity studies were performed in triplicate.

2.10 | Determination of Enzyme Inhibitory Activity

The inhibitory potential of *L. orientalis* extracts against urease and tyrosinase enzymes was assessed following previously reported protocols [37, 38]. Kojic acid was used as the positive control for tyrosinase inhibition, while thiourea served as the standard for urease inhibition. Enzyme inhibition capacity was expressed as IC_{50} values (μg/mL), representing the concentration required to achieve 50% inhibition. The enzyme inhibitory assay was performed in triplicate.

2.11 | In Vitro Scratch Wound Closure Assay

The wound healing potential of the extracts was evaluated by the in vitro scratch assay, a commonly used in vitro method for evaluating scratch/gap closure under controlled conditions [39]. Experiments were conducted on healthy human embryonic kidney 293T (HEK-293T) cells. The cells were seeded into Petri dishes at a density of 1×10^4 cells per well. After 24 h of incubation, a scratch was created in the cell monolayer using a sterile scriber to mimic a wound. The medium was then replaced with fresh medium containing the extracts, and cells were further incubated at 37°C under a 5% CO_2 atmosphere. Wound closure was assessed by monitoring scratch width at 0, 24, 48, and 72 h. The assay was performed in triplicate.

2.12 | Cytotoxicity Assay

The cytotoxicity of *L. orientalis* extracts was evaluated on HEK-293T cells using the MTT assay [40]. Cells were seeded into 96-well plates at a density of 1×10^4 cells per well in triplicate and maintained at 37°C in a humidified atmosphere (5% CO_2, 95% air). After cell attachment, extracts were applied at six concentrations ranging from 25 to 800 μg/mL. Following 72 h of incubation, MTT solution was added to each well, and absorbance was recorded at 540 nm with a microplate reader. Cell viability was expressed as a percentage relative to untreated control cells.

2.13 | Preparation of PVA/Starch Hydrogel Films

Hydrogel films were fabricated by solution casting, following the procedure of Altaf et al. (2021) with minor adjustments [41]. A 10% (w/v) PVA solution was prepared by stirring at 80°C for 2 h, while a 7% starch solution was obtained by stirring at 100°C for 20 min. The extracts (5% w/w) were incorporated into the starch solution and then combined with the PVA solution. Subsequently, 10 mL of ethanol, 0.5 mL of glutaraldehyde, 0.05 mL of dilute HCl, and 2 mL of glycerol were added to the polymer mixture. In this formulation, glutaraldehyde served as the cross-linking agent, dilute HCl provided the acidic catalytic conditions for cross-linking, ethanol acted as a co-solvent/medium component, and glycerol was used as a plasticizer. Films were cast and dried at room temperature for 48 h. After drying, the hydrogel films were detached from the Petri dishes and stored in airtight bags to prevent contamination.

2.14 | Preparation of PVA/Chitosan Hydrogel Films

PVA/chitosan composite films loaded with *L. orientalis* extracts were obtained by solvent casting [42]. A 9% (w/w) PVA solution was stirred at 80°C for 2 h and blended with a 2% chitosan solution prepared in dilute acetic acid. Extracts (5% w/w) were added to this solution until homogenized. Cross-linking was achieved by adding 0.1 mL glutaraldehyde in 0.1 mL HCl. The final mixture was cast into Petri dishes, dried at room temperature for 48 h, and stored in sealed bags.

2.15 | Preparation of Chitosan/Gelatin Hydrogel Films

Chitosan/gelatin films were prepared following Patel et al. (2018) with modifications [11]. Chitosan solution (2%) was dissolved in 1% acetic acid with 0.3 mL glycerol added as a plasticizer. A 2.5% (w/v) gelatin solution was separately prepared in distilled water, and 0.7 mL of glycerol was added under continuous stirring until a homogeneous mixture was obtained. The gelatin and chitosan solutions were mixed at 40°C for 6 h, followed by the addition of 3 mL of 0.25% glutaraldehyde. Extracts (5% w/w) were then incorporated, and the mixture was stirred until uniform. Films were cast, dried for 48 h at room temperature, and stored in airtight bags.

2.16 | Preparation of Chitosan Hydrogel Films

Chitosan solution (2%) was prepared in 1% acetic acid, and 100 μL glycerol was added as a plasticizer and mixed. Extracts (5% w/w) were then incorporated, and the mixture was poured into Petri dishes. Films were dried in an oven at 30°C for 48 h and stored in sealed bags [43].

2.17 | Characterization of Hydrogel Films

Before physicochemical and biological evaluations, all hydrogel films were conditioned under identical laboratory conditions and cut into standardized dimensions according to each assay. Within each experiment, film samples with identical exposed surface areas were used. All extract-loaded formulations contained the same nominal extract loading ratio of 5% (w/w). For antioxidant and antimicrobial assays, square film pieces of the same dimensions were used, whereas 2 × 2 cm samples containing approximately 20 mg of extract were used for release studies. Although slight thickness differences may arise from variations in polymer composition and drying behavior, identical casting conditions, sample dimensions, extract loading ratios, and assay conditions were applied to ensure comparative evaluation among formulations.

2.17.1 | Scanning Electron Microscopy (SEM) Analysis

The surface morphology of the prepared hydrogel films was investigated by scanning electron microscopy (SEM). Images were captured using a FEI Quanta 650 FEG instrument (ÇÜMERLAB, Çukurova University, Turkey) under high-vacuum operating conditions.

2.17.2 | Fourier Transform Infrared (FT-IR) Spectroscopy Analysis

The chemical functionalities of the pure extracts, blank hydrogel films, and extract-loaded hydrogel films were examined by Fourier transform infrared spectroscopy (FT-IR). Spectra were recorded using a Thermo Scientific Nicolet iS10 FT-IR spectrometer equipped with an attenuated total reflectance (ATR) accessory (Thermo Fisher Scientific, Waltham, MA, USA). Measurements were performed in the spectral range of 4000–400 cm^{-1} at a resolution of 4 cm^{-1}, and 32 scans were averaged for each sample. The spectra of LOLE and LORE were also recorded and compared with those of the corresponding blank and extract-loaded hydrogel films to support the evaluation of extract incorporation and possible intermolecular interactions.

2.17.3 | Swelling Behavior

The swelling behavior of hydrogel films was evaluated by immersing pre-weighed (1 × 1 cm) dried samples (W_0) in phosphate-buffered saline (PBS, pH 7.4) at 37°C. After 24 h, the swollen samples were removed, gently blotted with filter paper to remove excess surface water, and immediately weighed (W_t) [43]. The swelling ratio (SR) was calculated using the following equation:

$$SR\,(\%) = \frac{W_t - W_0}{W_0} \times 100 \quad (1)$$

The swelling test was performed in triplicate for each formulation.

2.17.4 | Degradation Studies

The degradation behavior of the hydrogels was assessed by monitoring weight loss over time in physiological conditions [44]. Dried hydrogel samples were weighed (W_0) and incubated in PBS (pH 7.4) at 37°C under gentle shaking (150 rpm). At specific time intervals (6th, 9th, and 14th days), samples were removed, washed with distilled water to eliminate residual salts, freeze-dried, and reweighed (W_t). The percentage of weight loss was calculated using the following equation:

$$Weight\ loss\ (\%) = \frac{W_0 - W_t}{W_0} \times 100 \quad (2)$$

Degradation studies were performed in triplicate for each formulation.

2.17.5 | In Vitro Release

For the in vitro release studies, hydrogel films (2 × 2 cm) containing approximately 20 mg of extract were immersed in 40 mL of phosphate buffer solutions at pH 7.4 and pH 5.5 and agitated at 150 rpm. Samples were collected at specific time intervals and replaced with the same volume of fresh buffers. The collected samples were passed through a polyvinylidene fluoride (PVDF) cartridge and subsequently analyzed by HPLC-DAD or UV spectrophotometer [45]. The release data were expressed as the cumulative percentage release of the compounds.

Release experiments were performed in triplicate for each formulation and pH condition, and the results were expressed as mean ± standard deviation (SD). To evaluate the release mechanism, the cumulative release data were fitted to zero-order, first-order, Higuchi, and Korsmeyer–Peppas kinetic models [46]. The goodness of fit was assessed using the coefficient of determination (R^2). For the Korsmeyer–Peppas model, the initial release portion corresponding to $Mt/M\infty \leq 0.60$ was used to estimate the release exponent (n), where $Mt/M\infty$ represents the fraction of extract released at time t, Mt is the amount of extract released at time t, and $M\infty$ is the total amount released at equilibrium.

2.18 | Statistical Analysis

All experimental data were obtained from triplicate measurements or independently prepared samples, as specified in the corresponding methodological sections. Results are presented as mean ± standard deviation (SD). Statistical analyses were performed using one-way analysis of variance (ANOVA), followed by Tukey's post hoc multiple-comparison test. For release studies, release percentages obtained at pH 5.5 and pH 7.4 were statistically compared at corresponding time points for each formulation using Welch's t-test. Differences were considered statistically significant at $p < 0.05$.

3 | Results and Discussion

3.1 | Total Phenolic and Flavonoid Contents

Total phenolic and flavonoid contents of *L. orientalis* leaf and resin extracts were determined as pyrocatechol and quercetin equivalents (mg/g), respectively (Table 1). The alcoholic extract of *L. orientalis* leaves (224.3 ± 0.35 mg PEs/g) contained higher levels of total phenolic compounds compared to the resin extract (102.8 ± 0.58 mg PEs/g). Regarding flavonoids, the alcoholic leaf extract contained 90.42 ± 0.12 mg QEs/g, whereas no flavonoids were detected in the resin extract. These findings indicate that the ethanol extract of *L. orientalis* leaves is richer in both total phenolic and flavonoid contents compared to the resin extract.

In the literature studies, the total phenolic content of the ethanol extract of *L. orientalis* leaves was found to contain 333.14 ± 7.96 mg GAE/g extract [22]. In another study, the methanol extract of *L. orientalis* leaves exhibited 42.30 ± 0.04 mg GAE/g total phenolics and 25.02 ± 0.66 mg QE/g total flavonoids, while the methanol

TABLE 1 | Antioxidant activity and total phenolic-flavonoid content of the extracts of *Liquidambar orientalis*.

Antioxidant Activity								
Plant	Extracts	β-carotene-linoleic acid assay IC_{50} (μg/mL)	DPPH˙ assay IC_{50} (μg/mL)	$ABTS^{\cdot+}$ assay IC_{50} (μg/mL)	CUPRAC assay $A_{0.50}$ (μg/mL)	Metal chelating assay IC_{50} (μg/mL)	Total phenolic content (mg PEs / g extract)	Total flavonoid content (mg QEs / g extract)
L. orientalis	LORE	54.26 ± 0.90	65.44 ± 0.74	34.70 ± 0.28	65.28 ± 0.51	93.05 ± 0.76	102.8 ± 0.58	*NA*
	LOLE	10.41 ± 0.66	16.14 ± 0.60	10.25 ± 0.34	21.59 ± 0.15	77.43 ± 0.57	224.3 ± 0.35	90.42 ± 0.12
Standards	BHA	1.40 ± 0.01	19.70 ± 0.18	12.80 ± 0.50	25.17 ± 0.01	*NT*	*NT*	*NT*
	α-tocopherol	2.20 ± 0.04	38.75 ± 0.23	34.50 ± 0.47	85.41 ± 0.01	*NT*	*NT*	*NT*
	EDTA	*NT*	*NT*	*NT*	*NT*	5.40 ± 0.21	*NT*	*NT*

IC_{50} and $A_{0.50}$ values represent the means ± SD of three parallel measurements ($p<0.05$). BHA, α-tocopherol, and EDTA were used as reference compounds. NA: not available, NT: not tested

extract of *L. orientalis* balsam contained 43.37 ± 0.10 mg GAE/g phenolics and 8.60 ± 0.66 mg GAE/g flavonoids [47]. To date, no reports have evaluated the total flavonoid content of *L. orientalis* leaves or the phenolic/flavonoid composition of the resin.

3.2 | Phenolic Composition

The phenolic composition of LOLE and LORE is presented in Table 2. Among the 26 phenolic compound standards screened, eleven were detected in the LOLE and eight in the LORE. Myricetin (37.50 mg/g) was identified as the major compound in the LOLE, followed by gallic acid (19.83 mg/g), trans-cinnamic acid (9.65 mg/g), and quercetin (6.36 mg/g). In contrast, *trans*-cinnamic acid (97.63 mg/g) was the predominant compound in the LORE. Trans-cinnamic acid, gallic acid, caffeic acid, vanillin, and *p*-coumaric acid were common to both extracts.

Myricetin, one of the most studied polyphenols detected in *L. orientalis* leaves, is reported to exert diverse biological activities including anticancer, anti-inflammatory, antibacterial, wound healing, antioxidant, and antidiabetic effects [48–51]. Gallic acid, another abundant compound in the leaves, is known for its high antioxidant capacity due to its three hydroxyl groups and has also been associated with anti-inflammatory, antimicrobial, and anticancer properties [52, 53]. Trans-cinnamic acid, the major component in the resin, has been reported to possess antioxidant and antimicrobial activities and to promote fibroblast migration during wound healing [54, 55].

In a previous study, protocatechuic acid (12.23 mg/g extract), (−)-epicatechin (7.95 mg/g extract), and gallic acid (3.26 mg/g extract) were identified as major constituents in the ethanol extract of *L. orientalis* leaves [22]. Additionally, several phenolic compounds such as styrene, phenylpropyl alcohol, cinnamyl alcohol, cinnamic acid, phenylpropyl cinnamate, and styracin were reported in the resin [13].

These findings highlight the distinct phenolic composition of *L. orientalis* leaves and resin, underlining their potential pharmacological relevance and providing a valuable basis for future bioactivity-oriented investigations.

3.3 | Antioxidant Activity

Free radicals and reactive oxygen species (ROS) generated during oxidative processes in wounds cause cellular damage and apoptosis, ultimately delaying or impairing wound healing. Therefore, antioxidants play a crucial role in preventing excessive ROS production at the wound site and in promoting rapid tissue repair [56]. The antioxidant activities of LOLE and LORE were evaluated using five different assays, and the results are summarized in Table 1. In all assays, the LOLE exhibited the strongest antioxidant activity. Specifically, the LOLE showed higher activity than both α-tocopherol and BHA in DPPH (IC_{50}: 16.14 ± 0.60 μg/mL), ABTS (IC_{50}: 10.25 ± 0.34 μg/mL), and CUPRAC ($A_{0.50}$: 21.59 ± 0.15 μg/mL) assays. In contrast, the LORE consistently displayed lower activity compared to the leaf extract. Additionally, LORE (IC_{50}: 34.70 ± 0.28 μg/mL) also demonstrated comparable activity to α-tocopherol (IC_{50}: 34.50 ± 0.47 μg/mL) in the ABTS radical scavenging assay.

TABLE 2 | Phenolic composition of LORE and LOLE determined by HPLC-DAD. (mg/g).

No	Phenolic compounds[a]	RT (min)	LORE	LOLE
1	Gallic acid	5.62	1.31 ± 0.08	19.83 ± 0.48
2	Protocatechuic acid	8.82	—[b]	4.48 ± 0.22
3	Catechin	10.71	—	0.91 ± 0.03
4	Pyrocatechol	11.04	—	—
5	Chlorogenic acid	12.35	—	—
6	p-hydroxy benzoic acid	12.72	1.59 ± 0.05	—
7	6,7-dihydroxy coumarin	14.10	—	—
8	Caffeic acid	15.17	3.86 ± 0.12	0.75 ± 0.04
9	3-hydroxy benzoic acid	15.98	—	—
10	Syringic acid	16.56	—	—
11	Vanillin	17.83	3.37 ± 0.15	3.44 ± 0.19
12	*p*-Coumaric acid	20.60	6.42 ± 0.17	4.79 ± 0.56
13	Taxifolin	21.26	—	—
14	Ferulic acid	22.14	—	—
15	Coumarin	24.49	—	—
16	Rutin	25.34	—	4.33 ± 0.22
17	Ellagic acid	25.98	2.44 ± 0.10	—
18	Rosmarinic acid	26.49	0.81 ± 0.05	—
19	Myricetin	27.25	—	37.50 ± 0.82
20	Quercetin	30.85	—	6.36 ± 0.25
21	*trans*-cinnamic acid	31.42	97.53 ± 0.55	9.65 ± 0.33
22	Luteolin	31.68	—	—
23	Hesperetin	32.25	—	—
24	Kaempferol	33.21	—	1.05 ± 0.08
25	Apigenin	33.80	—	—
26	Chrysin	33.17	—	—

[a]Values expressed are means ± SD of three parallel measurements.
[b]not detected.

The lower antioxidant activity of LORE compared with LOLE can be mainly attributed to differences in their phytochemical composition. LOLE contained a markedly higher total phenolic content and detectable flavonoids, whereas LORE showed lower total phenolic content and no detectable flavonoid content. In addition, HPLC-DAD analysis revealed that LOLE was rich in myricetin, gallic acid, quercetin, and other hydroxylated phenolic compounds, which are well known for their hydrogen- or electron-donating capacity. By contrast, LORE was dominated by trans-cinnamic acid, a phenylpropanoid with antimicrobial relevance but comparatively fewer hydroxyl groups contributing to radical scavenging [57]. Therefore, the stronger antioxidant performance of LOLE is most likely related to its higher abundance and diversity of polyphenolic/flavonoid constituents.

Previous studies support these findings. Saraç and Şen (2014) reported that ethanol extracts of *L. orientalis* leaves exhibited DPPH radical scavenging activity with an IC_{50} of 3.11 ± 0.024 mg/mL and a total antioxidant capacity (β-carotene–linoleic acid assay) of 96.55% ± 0.54% at 20 mg/mL [22]. Similarly, Çetinkaya et al. (2022) found that the methanol extract of *L. orientalis* leaves had a DPPH IC_{50} of 43.63 ± 1.12 µg/mL, while the methanol extract of balsam displayed an IC_{50} of 56.40 ± 2.19 µg/mL [47]. In another study, Baloglu et al. (2023) reported the antioxidant activity of *L. orientalis* gum, with DPPH and ABTS scavenging activities of 45.69 ± 0.05 and 15.56 ± 0.37 mg TE/g gum, respectively, as well as CUPRAC and FRAP activities of 94.60 ± 1.95 and 47.89 ± 0.31 mg TE/g gum [58].

Overall, these results indicate that *L. orientalis* leaves are a particularly rich source of natural antioxidants with higher activity than the resin, highlighting their potential role in wound healing applications.

3.4 | Antimicrobial Activity

In wound healing, the colonization of microorganisms on the wound surface often results in infection, which significantly delays the healing process [59]. In such cases, antimicrobial

TABLE 3 | Minimum inhibitory concentrations (MIC) of the LOLE and LORE against tested microorganisms (mg/mL).

Plant	Extracts	*S. aureus*	*B. subtilis*	*E. coli*	*P. aeruginosa*	*E. aerogenes*	*C. albicans*
		MIC value (mg/mL)					
L. orientalis	LORE	0.625	0.156	1.25	5	2.5	0.625
	LOLE	2.5	2.5	2.5	10	2.5	1.25

MIC values are expressed as the lowest concentration that completely inhibited visible microbial growth in the broth microdilution assay. Experiments were performed in triplicate, and the reported MIC values correspond to the consistently observed inhibitory concentrations.

agents are required to prevent or control infection [60]. The antimicrobial activities of LOLE and LORE were evaluated against clinically relevant skin pathogens, including Gram-negative *Pseudomonas aeruginosa*, *Escherichia coli*, and *Enterobacter aerogenes*; Gram-positive *Bacillus subtilis* and *Staphylococcus aureus*; and the yeast *Candida albicans*. Minimum inhibitory concentration (MIC) values of the extracts are summarized in Table 3. Overall, LORE exhibited stronger antimicrobial activity than LOLE. The LOLE inhibited the growth of all tested microorganisms with MIC values ranging from 1.25 to 10 mg/mL, while the LORE inhibited the same microorganisms with MIC values ranging from 0.156 to 5 mg/mL. LORE displayed the lowest MIC against *B. subtilis* (0.156 mg/mL), followed by *C. albicans*, *S. aureus* (0.625 mg/mL), and *E. coli* (1.25 mg/mL). LOLE showed the best effect against *C. albicans* with an MIC value of 1.25 mg/mL.

The stronger antimicrobial activity of LORE compared with LOLE can be explained by its distinct resinous phytochemical composition. HPLC-DAD analysis showed that LORE was dominated by trans-cinnamic acid, which has been associated with antimicrobial effects against various microorganisms [61]. In addition, resin-derived phenylpropanoid and relatively hydrophobic constituents may interact more efficiently with microbial cell membranes, leading to increased membrane permeability and growth inhibition [62]. In contrast, LOLE contained higher amounts of polar phenolic and flavonoid compounds, which contributed more prominently to antioxidant activity but may exhibit comparatively weaker direct antimicrobial effects. Therefore, the superior antimicrobial activity of LORE is most likely related to the high abundance of trans-cinnamic acid and the membrane-interactive nature of resin-associated constituents.

These results are partly consistent with previous reports. Okmen et al. (2014) demonstrated that ethanol extracts of *L. orientalis* leaves exhibited notable antimicrobial activity, with MIC values of 1625 µg/mL against *B. subtilis*, *S. aureus*, and *Enterococcus faecalis*, and 3250 µg/mL against *Listeria monocytogenes*, *E. coli*, *Yersinia enterocolitica*, *Salmonella typhimurium*, and *C. albicans* [19]. Avunduk and Kaçar (2013) further reported that methanol extracts of *L. orientalis* resin produced inhibition zones ranging from 8 to 12 mm against eight pathogenic microorganisms, with the largest zone observed against *E. coli* [63].

Collectively, these findings demonstrate that *L. orientalis* resin possesses stronger antimicrobial activity than the leaf extract, supporting its potential as a natural antimicrobial agent for managing wound-associated infections.

3.5 | Biofilm Inhibition

In chronic and burn wounds, biofilm formation hinders treatment and delays the healing process. In this study, the antibiofilm activities of LORE and LOLE were evaluated against a panel of Gram-positive, Gram-negative, and fungal strains at different concentrations (MIC to MIC/8). The results demonstrated a clear dose-dependent trend, with the highest inhibition observed at MIC levels and a gradual decline toward MIC/8 (Table 4).

LORE exhibited the strongest antibiofilm activity against *S. aureus*, with an inhibition of 81.79% ± 2.35% at the MIC concentration, whereas LOLE achieved 60.21% ± 2.58% inhibition at the same level. At lower concentrations, LORE inhibited biofilm formation by 63.26% ± 1.50% (MIC/2) and 48.59% ± 1.75% (MIC/4). Similarly, against *B. subtilis*, LORE achieved 65.78% ± 2.10% inhibition, followed by LOLE with 58.27% ± 1.65%.

LORE also inhibited biofilm formation by 55.22% ± 1.15% against *C. albicans* at the MIC concentration. In the case of *E. coli*, LORE and LOLE demonstrated inhibition rates of 63.72% ± 2.21% and 46.39% ± 1.86%, respectively. By contrast, the lowest activities were recorded against *P. aeruginosa*, with inhibition values of only 42.15% for LORE and 35.57% for LOLE at MIC. Against *E. aerogenes*, LORE and LOLE exhibited inhibition rates of 71.39% ± 1.75% and 55.56% ± 1.70%, respectively.

To the best of our knowledge, this is the first report describing the antibiofilm potential of *L. orientalis* extracts. These findings provide novel evidence of biofilm inhibition by this species and highlight the wound-healing potential of both resin and leaf extracts.

3.6 | Anti-QS Activity

The quorum-sensing (QS) inhibitory activities of LOLE and LORE were evaluated through multiple complementary assays. In the *C. violaceum* CV026 biosensor strain, the MIC values of LORE and LOLE were determined as 5 and 2.5 mg/mL, respectively. Both extracts produced clear inhibition zones at MIC and sub-MIC concentrations. At MIC, LORE exhibited a larger inhibition zone (17.0 mm) than LOLE (12.0 mm). Even at MIC/2, LORE (13.5 mm) maintained a stronger effect compared to LOLE (9.0 mm), indicating a more pronounced interaction with AHL-mediated signaling (Table S1).

For *C. violaceum* CV12472, the MIC values were 10 mg/mL for LORE and 5 mg/mL for LOLE. At MIC, both extracts completely

TABLE 4 | Antibiofilm activity of LOLE and LORE against tested microorganisms, expressed as biofilm inhibition (%).

Microorganisms	Extracts	Biofilm inhibition %			
		MIC	MIC/2	MIC/4	MIC/8
S. aureus	LORE	81.79 ± 2.35	63.26 ± 1.50	48.59 ± 1.75	25.41 ± 0.76
	LOLE	60.21 ± 2.58	40.26 ± 1.90	28.80 ± 1.56	16.80 ± 2.20
B. subtilis	LORE	65.78 ± 2.10	47.35 ± 1.58	31.52 ± 0.90	16.86 ± 1.24
	LOLE	58.27 ± 1.65	36.04 ± 1.22	21.90 ± 1.56	11.34 ± 1.15
C. albicans	LORE	55.22 ± 1.15	38.94 ± 1.70	26.36 ± 1.52	—
	LOLE	39.76 ± 2.31	23.81 ± 1.82	—	—
E. coli	LORE	63.72 ± 2.21	43.88 ± 1.85	28.85 ± 1.93	17.20 ± 0.95
	LOLE	46.39 ± 1.86	25.66 ± 1.38	14.83 ± 1.72	—
P. aeruginosa	LORE	42.15 ± 1.79	29.25 ± 1.28	15.46 ± 1.55	9.44 ± 1.32
	LOLE	35.57 ± 1.78	20.07 ± 1.21	10.76 ± 1.64	—
E. aerogenes	LORE	71.39 ± 1.75	58.12 ± 2.23	41.53 ± 1.59	27.93 ± 1.35
	LOLE	55.56 ± 1.70	31.02 ± 1.32	19.82 ± 0.95	11.62 ± 1.27

Values are expressed as biofilm inhibition (%) and presented as mean ± SD of three parallel measurements

inhibited violacein production. At sub-MIC concentrations, violacein synthesis was also markedly suppressed, with LOLE (75.5% inhibition at MIC/2) being more effective than LORE (66.1% at MIC/2) (Table S2).

Motility inhibition assays demonstrated that LORE was more effective than LOLE in suppressing the motility of *P. aeruginosa*. At 100 μg/mL, LORE inhibited swimming and swarming by 39.46% and 64.29%, respectively, whereas LOLE achieved 32.77% swimming and 53.57% swarming inhibition at the same concentration (Table S3).

These results suggest that by interfering with quorum sensing and motility, LORE and LOLE may reduce biofilm-associated infections, thereby contributing to an enhanced wound-healing process.

3.7 | In Vitro Scratch Wound Closure Assay

The in vitro scratch wound closure assay was performed to preliminarily evaluate the effect of LOLE and LORE on gap closure using HEK-293T cells (Figure 1). Compared with the untreated control, both extracts promoted faster closure of the scratched area under the tested conditions. After 24 h, LORE- and LOLE-treated cultures showed approximately 60% and 50% scratch closure, respectively, whereas the control group showed only 20% closure. At 48 h, scratch closure reached approximately 80% for LORE and 70% for LOLE, compared with 50% in the control. After 72 h, the scratched area was almost completely closed in the extract-treated groups, while the control group remained partially open (Figure 1).

These findings suggest that LOLE and LORE may enhance in vitro gap closure in HEK-293T cells. However, the scratch assay does not distinguish between cell migration and proliferation, and therefore the observed closure should not be interpreted as direct evidence of a specific cellular mechanism. In addition, HEK-293T cells are not skin-derived cells; thus, this assay should be considered a preliminary screening model rather than a physiologically complete wound-healing model. Further studies using skin-relevant cell types, such as dermal fibroblasts and keratinocytes, as well as in vivo wound models, are required to confirm the wound-healing potential of these extracts and extract-loaded hydrogel systems.

Although sweetgum resin has traditionally been used for the treatment of wounds, burns, and various skin disorders, scientific evidence supporting these traditional applications remains limited. Previous studies have mainly focused on sweetgum resin or storax-containing formulations [64], whereas the wound-related potential of *L. orientalis* leaf extract has been less explored. Recently, Cakmak et al. reported that sweetgum balsam-loaded poly(L-lactic acid)/chitosan scaffolds enhanced in vitro wound closure compared with controls [24]. In this context, the present findings provide preliminary evidence that both LOLE and LORE can promote scratch closure under the tested in vitro conditions, but further validation in skin-specific cellular and animal wound models is necessary.

3.8 | Cytotoxicity Assay

The cytotoxicity of LOLE and LORE was evaluated using the MTT assay on HEK-293T cells after 72 h of exposure (Figure S1). Cell viability remained relatively high for both extracts under the tested concentration range. Even at the highest tested concentration (400 μg/mL), LOLE and LORE maintained cell viability values of 85.50% and 77.38%, respectively. These results indicate that both extracts showed no apparent cytotoxicity toward HEK-293T cells under the tested conditions.

The cytotoxicity results support the preliminary biological suitability of LOLE and LORE for further evaluation in wound dressing formulations. However, these findings should not be interpreted as definitive evidence of biocompatibility or clinical

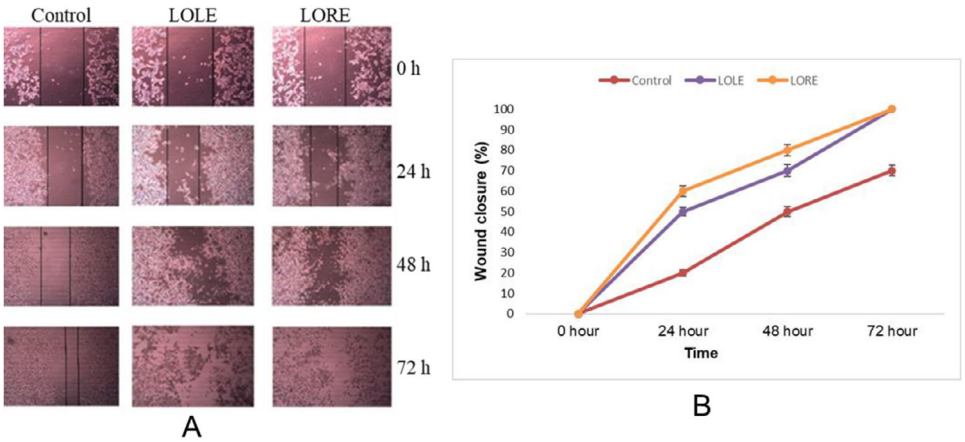


FIGURE 1 | (A) Microscopic images showing the in vitro scratch wound closure activity of LORE and LOLE on HEK-293T cells; (B) Percentage of wound closure in HEK-293T cells treated with LOLE and LORE at different incubation times.

TABLE 5 | Urease and tyrosinase inhibitory activities of *Liquidambar orientalis* leaf and resin extracts.

		Urease inhibitory activity	Tyrosinase inhibitory activity
Plant name	**Ethanol Extracts**	**IC_{50} (μg/mL)**	**IC_{50} (μg/mL)**
L. orientalis	LORE	45.21 ± 0.56	20.18 ± 0.35
	LOLE	80.39 ± 0.63	140.74 ± 1.05
Standards	Thiourea	9.05 ± 0.20	NT
	Kojic acid	NT	23.51 ± 0.28

IC_{50} values represent the means ± SD of three parallel measurements ($p<0.05$). Thiourea and kojic acid were used as reference compounds. NT: not tested.

safety, since only one non-skin-derived cell line was used. Additional cytotoxicity and compatibility studies using skin-relevant cells, including fibroblasts and keratinocytes, together with in vivo assessments, are required before stronger conclusions can be drawn regarding biomedical safety and wound dressing applicability.

3.9 | Enzyme Inhibitory Activity

Tyrosinase is a copper-containing enzyme that is widely found in nature and is responsible for melanin synthesis [65]. Excessive melanin production in the epidermis or dermis leads to skin darkening, a condition known as hyperpigmentation, which is associated with dermatological problems such as melasma, skin aging, and pigmentation disorders [66]. Hyperpigmentation is particularly evident during scar formation in severe wounds and burns [67]. In addition to cosmetic concerns, scar-related hyperpigmentation can adversely affect patients' quality of life.

The tyrosinase inhibitory activities of LOLE and LORE are shown in Table 5. LORE exhibited the strongest activity with an IC_{50} of 20.18 ± 0.35 μg/mL, which was comparable to that of kojic acid (IC_{50}: 23.51 ± 0.28 μg/mL), a widely used reference inhibitor. LOLE inhibited tyrosinase with an IC_{50} of 140.74 ± 1.05 μg/mL. To date, no studies have directly examined the tyrosinase inhibitory activity of *L. orientalis* leaves and resin. However, cinnamic acid—a key phenolic constituent of *L. orientalis*—has been reported to strongly inhibit tyrosinase. Kong et al. (2008) demonstrated that cinnamic acid inhibited tyrosinase activity by 13.1% and 70.6% at concentrations of 100 and 1000 μM, respectively [68]. Similarly, Shi et al. (2005) reported an IC_{50} value of 2.10 mM for cinnamic acid [69].

Helicobacter pylori is a gastric pathogen that survives the acidic stomach environment by producing urease, which hydrolyzes urea into ammonia and carbon dioxide. Excessive urease activity contributes to gastric ulcer, gastritis, and gastric cancer [70]. Due to antimicrobial resistance associated with conventional drugs, the search for novel urease inhibitors and antiulcer agents is ongoing [71]. The urease inhibitory activity of *L. orientalis* extracts is summarized in Table 5. LORE exhibited higher activity (IC_{50}: 45.21 ± 0.56 μg/mL) compared to LOLE (IC_{50}: 80.39 ± 0.63 μg/mL). Previous investigations have mainly focused on the in vivo antiulcerogenic effects of sweetgum balsam (Styrax liquidus) in rat models [18].

Taken together, both leaf and resin extracts of *L. orientalis* inhibited tyrosinase and urease enzymes, with the resin extract showing superior activity in both cases. These results suggest that *L. orientalis* resin may have dual therapeutic potential: contributing to scar-free wound healing through tyrosinase inhibition and providing gastroprotective effects through urease inhibition.

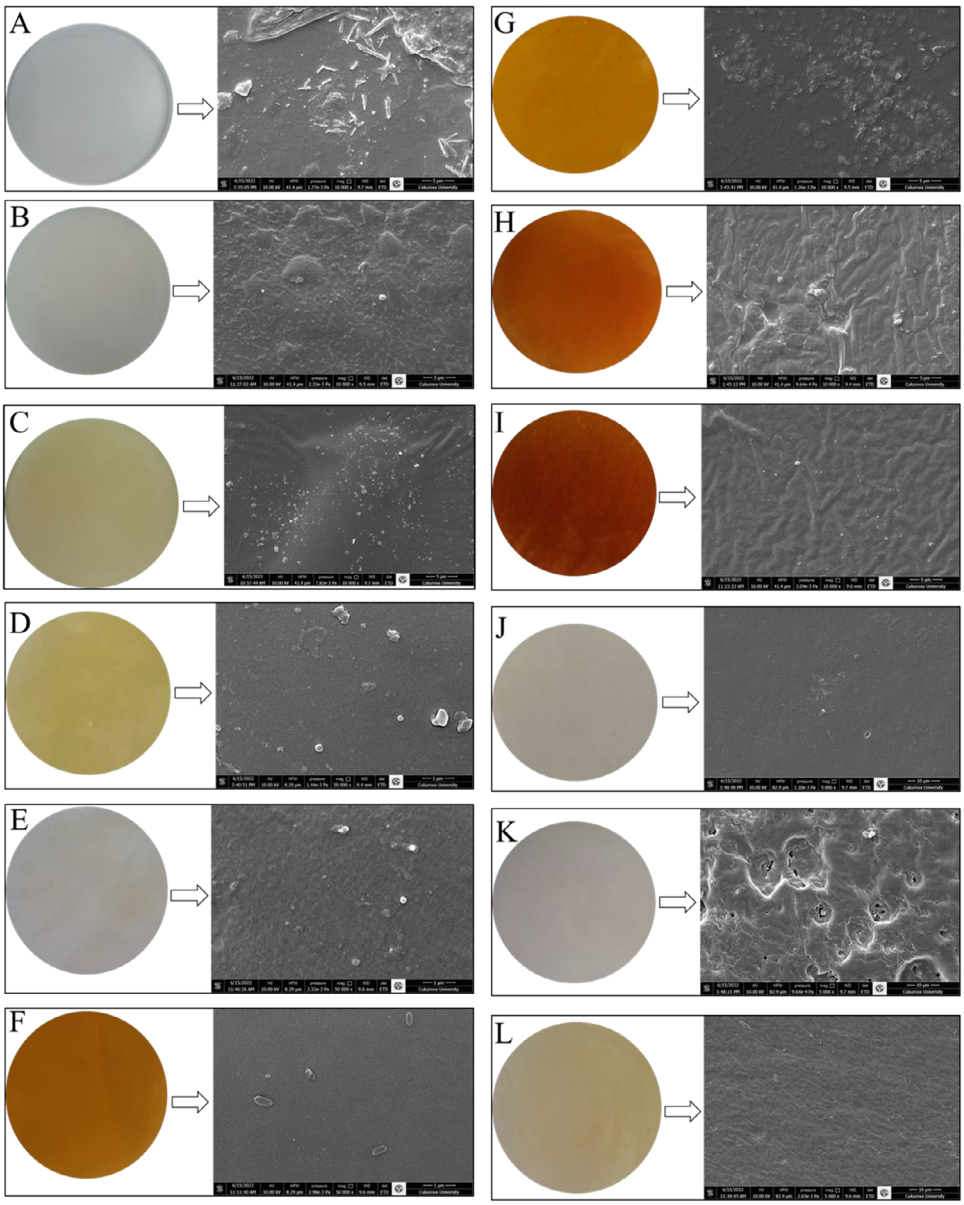


FIGURE 2 | SEM images of hydrogel films: (A) PVA/Starch (extract-free), (B) LORE-loaded PVA/Starch, (C) LOLE-loaded PVA/Starch, (D) Chitosan/Gelatin (extract-free), (E) LORE-loaded Chitosan/Gelatin, (F) LOLE-loaded Chitosan/Gelatin, (G) PVA/Chitosan (extract-free), (H) LORE-loaded PVA/Chitosan, (I) LOLE-loaded PVA/Chitosan, (J) Chitosan (extract-free), (K) LORE-loaded Chitosan, (L) LOLE-loaded Chitosan.

3.10 | Morphological Analysis

The surface morphology of PVA/starch, PVA/chitosan, chitosan/gelatin, and chitosan hydrogel films, both blank and loaded with LOLE or LORE extracts, was investigated by SEM. Morphological evaluation is critical to assess the relationship between extract incorporation and the structural properties of the films. Overall, the addition of extracts significantly altered the morphology of the hydrogel films.

In PVA/starch hydrogels, incorporation of LOLE resulted in the formation of dark channel-like structures (Figure 2), likely caused by the outward flow of water during drying. These channels are known to enhance fluid absorption and to facilitate extract release, thereby improving the functional properties of the film. In contrast, the addition of LORE led to surface fluctuations, reflecting interactions between the hydrogel matrix and the chemical constituents of the resin.

In chitosan/gelatin films, incorporation of LORE produced a slightly wavy and porous surface, whereas LOLE yielded a more homogeneous and compact morphology compared to the blank hydrogel (Figure 2). This smoothing effect may be attributed to the filling of voids within the hydrogel by the extract, which supports wound healing by promoting fibroblast and keratinocyte attachment [72].

The control PVA/chitosan films exhibited a heterogeneous porous surface, a result of water droplet evaporation during drying, which adversely affects mechanical stability [73]. Extract

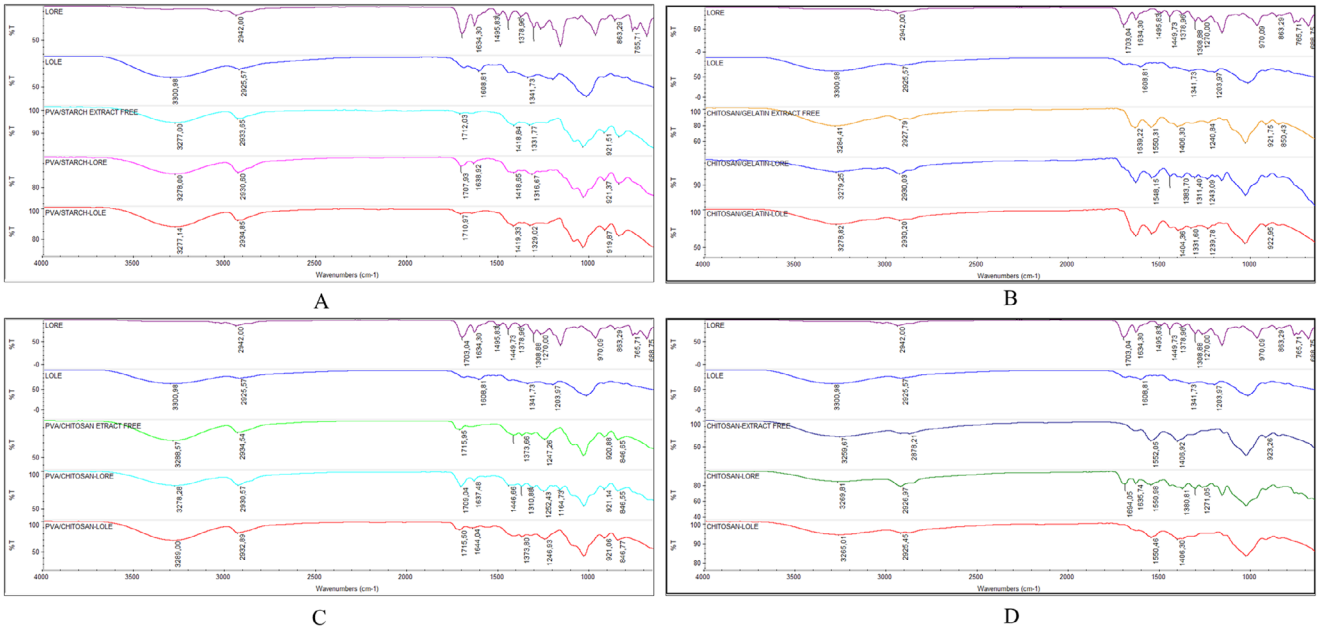


FIGURE 3 | FT-IR spectra of pure LOLE, pure LORE, and blank and extract-loaded hydrogel films: (A) PVA/starch, (B) Chitosan/gelatin, (C) PVA/chitosan, and (D) Chitosan films.

incorporation increased surface density and smoothed the film texture, suggesting successful loading [74]. Specifically, LOLE induced a wavy morphology, likely due to strong hydrogel interactions mediated by phenolic and flavonoid compounds, whereas LORE produced an irregular, wavy surface. The latter can be explained by hydrogen bonding between NH_2 and OH groups arising from the resin's chemical composition.

The initially smooth and uniform surface of the chitosan films became rougher upon extract incorporation. In the LOLE-loaded chitosan films, SEM images revealed slight ripples on the surface, indicating successful integration of the extract into the three-dimensional hydrogel network. In contrast, the incorporation of LORE resulted in a porous structure within the chitosan matrix, which can be attributed to the presence of apolar compounds in the resin's chemical composition.

Additionally, SEM images revealed that LOLE was entrapped within the three-dimensional hydrogel network, causing slight surface fluctuations. By contrast, the incorporation of LORE resulted in the formation of a porous structure, likely due to apolar components of the resin (Figure 2). Such porosity is advantageous in wound healing applications, as it enables efficient absorption of wound exudates and may accelerate tissue regeneration [75].

3.11 | FT-IR Analysis

FT-IR spectroscopy was used to evaluate the characteristic functional groups of the pure extracts, blank hydrogel films, and LOLE- or LORE-loaded hydrogel films, and to support the incorporation of the extracts into the polymeric matrices (Figure 3). It should be noted that FT-IR analysis alone does not unequivocally prove the formation of new covalent bonds between the extracts and polymer networks. Therefore, the spectral changes observed in this study were interpreted mainly as evidence of extract incorporation and possible intermolecular interactions, particularly hydrogen bonding and physical interactions, between extract constituents and polymer functional groups.

The FT-IR spectrum of LOLE showed characteristic bands associated with phenolic-rich plant extracts, including a broad absorption in the 3200–3400 cm^{-1} region corresponding to O—H stretching vibrations of phenolic hydroxyl groups. Bands in the 2920–2850 cm^{-1} region were attributed to aliphatic C—H stretching, while absorptions around 1600–1650 cm^{-1} and 1500–1600 cm^{-1} were associated with aromatic C═C stretching and/or carbonyl-related vibrations of phenolic constituents. Additional bands in the 1000–1300 cm^{-1} region were assigned to C—O stretching vibrations of phenolic acids, flavonoids, and alcohol groups. The LORE spectrum also displayed O—H and C—H stretching bands, together with characteristic absorptions attributable to aromatic and carboxylic groups of resin-associated phenylpropanoid compounds. In particular, the presence of trans-cinnamic acid as the major marker compound in LORE is consistent with bands related to aromatic C═C and carboxyl C═O/C—O vibrations.

In the PVA/starch control film, the broad band around 3277 cm^{-1} was assigned to overlapping O—H stretching vibrations of PVA, starch, and glycerol, reflecting extensive hydrogen bonding within the matrix. The band near 2933 cm^{-1} corresponded to aliphatic C—H stretching, while the absorption around 1712 cm^{-1} was attributed to residual carbonyl groups associated with partially hydrolyzed vinyl acetate units in PVA. The bands in the 1000–1150 cm^{-1} region were mainly related to C—O and C—O—C stretching vibrations of PVA and starch, consistent with previous reports on PVA/starch-based hydrogel films [41, 76]. After LOLE or LORE incorporation, broadening and slight intensity changes were observed in the O—H stretching region and, in

the C—O/C—O—C region, suggesting interactions between the hydroxyl-rich polymer network and phenolic or resin-associated constituents of the extracts.

In the PVA/chitosan control film, the broad absorption around 3277 cm^{-1} was attributed to overlapping O—H and N—H stretching vibrations from PVA and chitosan. The band around 2933 cm^{-1} corresponded to C—H stretching, while bands in the 1600–1650 cm^{-1} and 1500–1560 cm^{-1} regions were associated with amide I/amide II vibrations and N—H bending of chitosan. The bands around 1247–1331 cm^{-1} were assigned to C—N stretching, N—H bending, and C—H bending vibrations [42, 77]. Upon extract loading, changes in the intensity and width of the O—H/N—H region and minor shifts or intensity variations in the amide-related bands indicated possible hydrogen bonding between chitosan amino groups, PVA hydroxyl groups, and extract constituents. These changes were more evident in LOLE-loaded films, likely due to the abundance of phenolic hydroxyl groups in LOLE.

The chitosan/gelatin control film showed a broad band around 3284 cm^{-1}, corresponding to N—H and O—H stretching vibrations involved in hydrogen bonding. The bands near 1639 and 1550 cm^{-1} were attributed to amide I and amide II vibrations of gelatin and chitosan, including C═O stretching, N—H bending, and C—N stretching. The absorption bands in the 1000–1150 cm^{-1} region were related to C—O—C and C—O stretching vibrations of the polysaccharide backbone [11, 78]. After incorporation of LOLE or LORE, the amide I/amide II regions and the broad O—H/N—H stretching band showed changes in intensity and/or broadness. These spectral variations suggest possible intermolecular interactions between gelatin/chitosan functional groups and the phenolic or carboxyl-containing constituents of the extracts.

In the chitosan control film, the broad band in the 3200–3400 cm^{-1} region was assigned to O—H and N—H stretching vibrations, while the bands around 2920 cm^{-1} corresponded to C—H stretching. The absorptions in the 1600–1650 cm^{-1} and 1500–1560 cm^{-1} regions were attributed to amide I and amide II vibrations, respectively, and the bands around 1020–1080 cm^{-1} were assigned to C—O—C and C—O stretching of the chitosan backbone [79, 80]. Following extract incorporation, the O—H/N—H stretching band became broader and/or changed in intensity, while the amide-related and C—O stretching regions also showed minor variations. These changes support the interaction of LOLE and LORE constituents with chitosan chains, most likely through hydrogen bonding and electrostatic or physical interactions involving hydroxyl, amino, carbonyl, and carboxyl groups.

Overall, the FT-IR results indicated that the incorporation of LOLE and LORE into the hydrogel matrices caused detectable changes mainly in the O—H/N—H stretching, amide, carbonyl, and C—O/C—O—C regions. These changes were consistent with the presence of extract-derived phenolic, flavonoid, and phenylpropanoid constituents within the polymer networks [23]. However, since no distinct new bands unequivocally indicating covalent bond formation were observed, the results were interpreted as supporting extract incorporation and possible intermolecular interactions rather than confirming new chemical bond formation.

3.12 | Swelling Behavior of Hydrogel Films

The swelling behavior of hydrogel films is a critical property for wound dressing applications, as it enables the absorption of wound exudates and influences the hydration of the polymeric network, the diffusion of incorporated bioactive compounds, and the maintenance of a moist wound environment [81]. Overall, all hydrogel films exhibited increased swelling in PBS at pH 7.4 (Figure 4). Among the formulations, chitosan films displayed the highest swelling capacity after 24 h. Specifically, LOLE-loaded chitosan films reached a maximum swelling of 350%, whereas LORE-loaded chitosan films reached 215%. This marked difference indicates that extract composition strongly affected water uptake. The higher swelling capacity of LOLE-loaded films can be attributed to the hydrophilic and phenolic-rich composition of the leaf extract, which contains hydroxylated compounds capable of enhancing water affinity within the polymeric matrix. In contrast, the more resinous, oily, and relatively hydrophobic character of LORE likely reduced swelling by limiting matrix–water interactions.

Free chitosan films exhibited greater swelling than cross-linked hydrogels, probably due to their less constrained polymeric network and the absence of chemical cross-linking restrictions. The high swelling of chitosan-based films is consistent with previous studies reporting that chitosan-containing wound dressing materials can absorb substantial amounts of aqueous medium because of their hydrophilic amino and hydroxyl groups, ionic character, and ability to form hydrogen bonds with water [82]. Such swelling behavior is generally considered beneficial for wound dressings because it may support exudate uptake and help maintain a hydrated wound interface; however, excessive swelling should be balanced with sufficient structural integrity and mechanical stability [83].

Following chitosan films, chitosan/gelatin hydrogels showed the next highest swelling. This behavior can be explained by the combined contribution of hydrophilic functional groups in both polymers, including hydroxyl and amino groups in chitosan and amide/carboxyl groups in gelatin [84]. Hydrogen bonding between these groups and water molecules, together with possible electrostatic interactions between protonated amino groups of chitosan and negatively charged carboxylate groups of gelatin, may facilitate water uptake [84]. Similar observations have been reported for chitosan/gelatin-based hydrogel or film systems, where swelling is mainly governed by polymer hydrophilicity, ionic interactions, and network porosity [85].

In contrast, PVA/starch hydrogels exhibited the lowest swelling behavior among the tested matrices. Although both PVA and starch contain abundant hydroxyl groups, the formation of a denser hydrogen-bonded and cross-linked network can restrict polymer chain mobility and limit water penetration [86]. PVA/chitosan films also showed comparatively lower swelling than free chitosan films, suggesting that incorporation of PVA and cross-linking reduced the accessibility of hydrophilic groups and constrained the network. This trend agrees with previous reports showing that PVA-containing and cross-linked hydrogel systems generally display more controlled swelling due to increased network density and intermolecular interactions [81, 87].

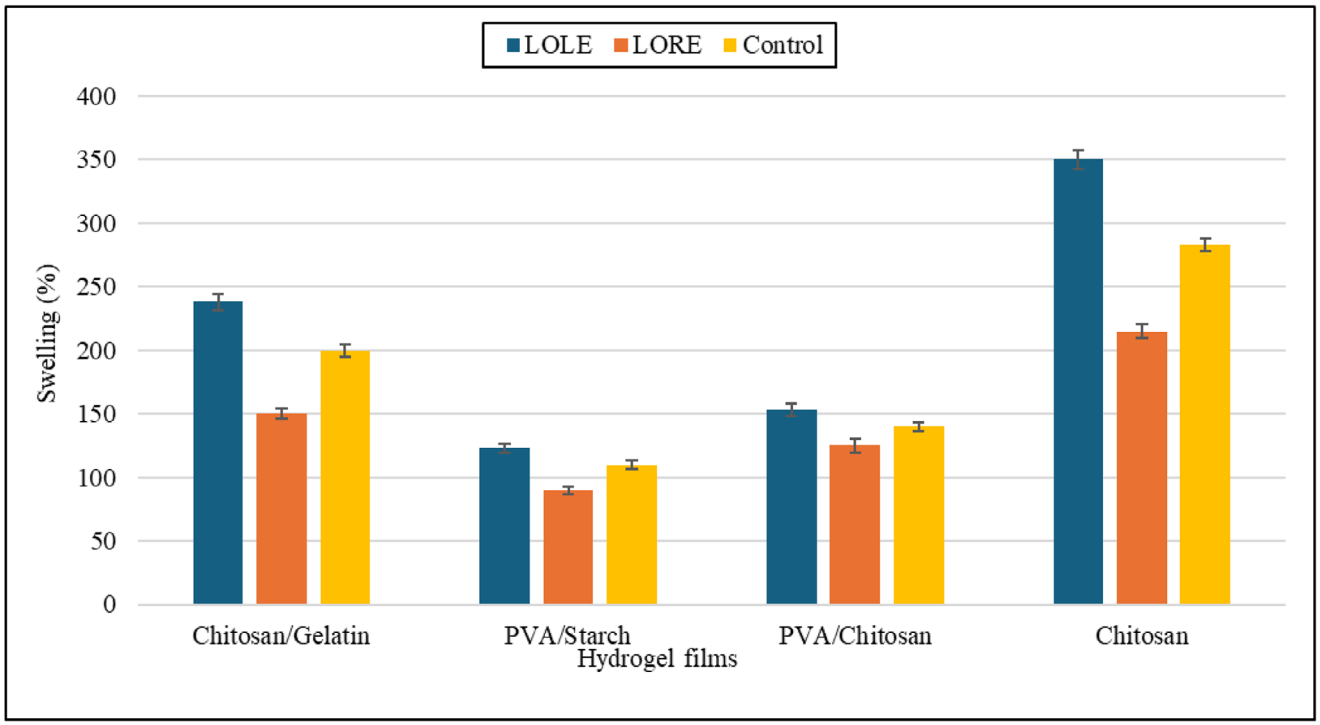


FIGURE 4 | Swelling behavior of different hydrogel films (PVA/starch, PVA/chitosan, Chitosan/gelatin, and Chitosan) in PBS at pH 7.4. Data are presented as mean ± SD ($n = 3$).

Taken together, the swelling results demonstrate that water uptake was governed by the combined effects of polymer composition, cross-linking, and extract characteristics. The higher swelling of LOLE-loaded chitosan films and the lower swelling of LORE-loaded and PVA-containing films are consistent with the expected structure–swelling relationships of these hydrogel matrices. These findings also help explain the release behavior observed in subsequent experiments, where more highly swollen chitosan-based films generally showed faster extract release than the more restricted PVA-containing matrices.

3.13 | In Vitro Degradation Analysis

The biodegradability of extract-loaded hydrogel films is a critical factor for their application as wound dressings and for evaluating their long-term stability [88]. Degradation was assessed by monitoring the weight loss of the films after incubation in PBS (pH 7.4) at room temperature for 14 days (Figure 5).

All hydrogel films showed progressive weight loss over time, with the degradation rate increasing up to day 14. In particular, LOLE-loaded chitosan and chitosan/gelatin films exhibited rapid degradation, losing more than 50% of their weight within the first six days. By day 14, the highest degradation was observed in LOLE-loaded chitosan films (87%), compared to 53% for LORE-loaded chitosan films and 70% for the control group.

Among the formulations, chitosan-based hydrogels degraded faster than the other systems, followed by chitosan/gelatin, PVA/chitosan, and PVA/starch films. The use of cross-linkers was found to reduce degradation, consistent with previous reports [89]. The slower degradation of LORE-loaded hydrogels compared to controls is likely due to apolar resin components that hinder dissolution in PBS.

Interestingly, the degradation trends were consistent with swelling behavior: films with higher swelling capacity also exhibited faster degradation. This relationship highlights the importance of balancing swelling and biodegradability in the design of hydrogel wound dressings.

3.14 | In Vitro Release Study

The release profiles of LOLE and LORE from hydrogel films were evaluated for 96 h in phosphate-buffered saline (PBS) at pH 5.5 and pH 7.4 (Figure 6). Release from LORE-loaded films was monitored by HPLC-DAD using trans-cinnamic acid as a marker compound, whereas release from LOLE-loaded films was quantified spectrophotometrically based on total phenolic content.

The pH values of 5.5 and 7.4 were selected to compare release behavior under mildly acidic wound-like conditions and near-physiological conditions, respectively. However, wound pH is dynamic and may vary depending on wound type, infection status, exudate composition, and healing stage [90, 91]. Therefore, the present results should be interpreted as pH-dependent release behavior within the tested pH range rather than as a comprehensive demonstration of responsiveness across the full pH spectrum of wounds. Additional pH values should be evaluated in future studies to more completely characterize the pH sensitivity of these hydrogel systems.

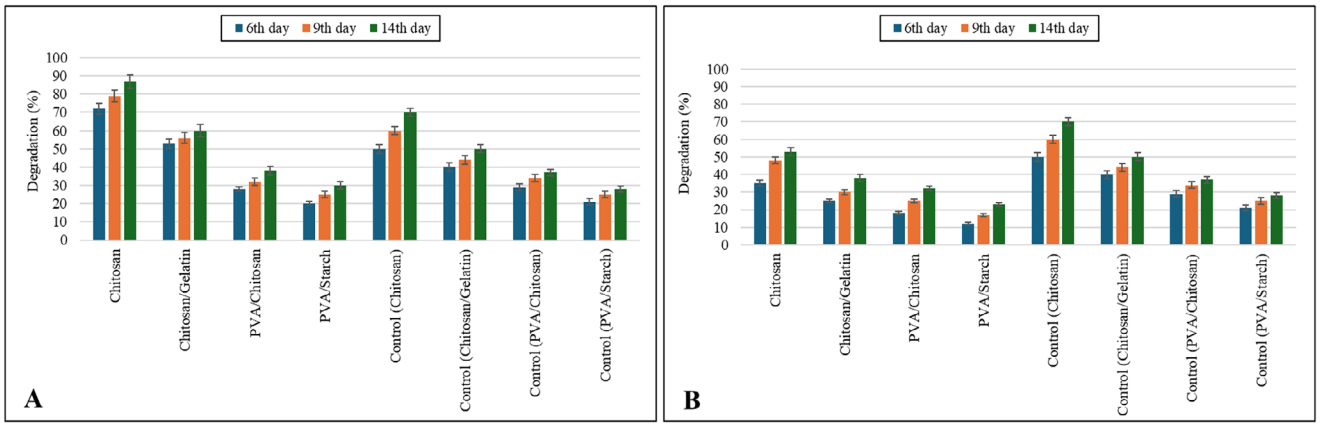


FIGURE 5 | in vitro degradation analysis of hydrogel films loaded with (A) LOLE and (B) LORE. Data are presented as mean ± SD ($n = 3$).

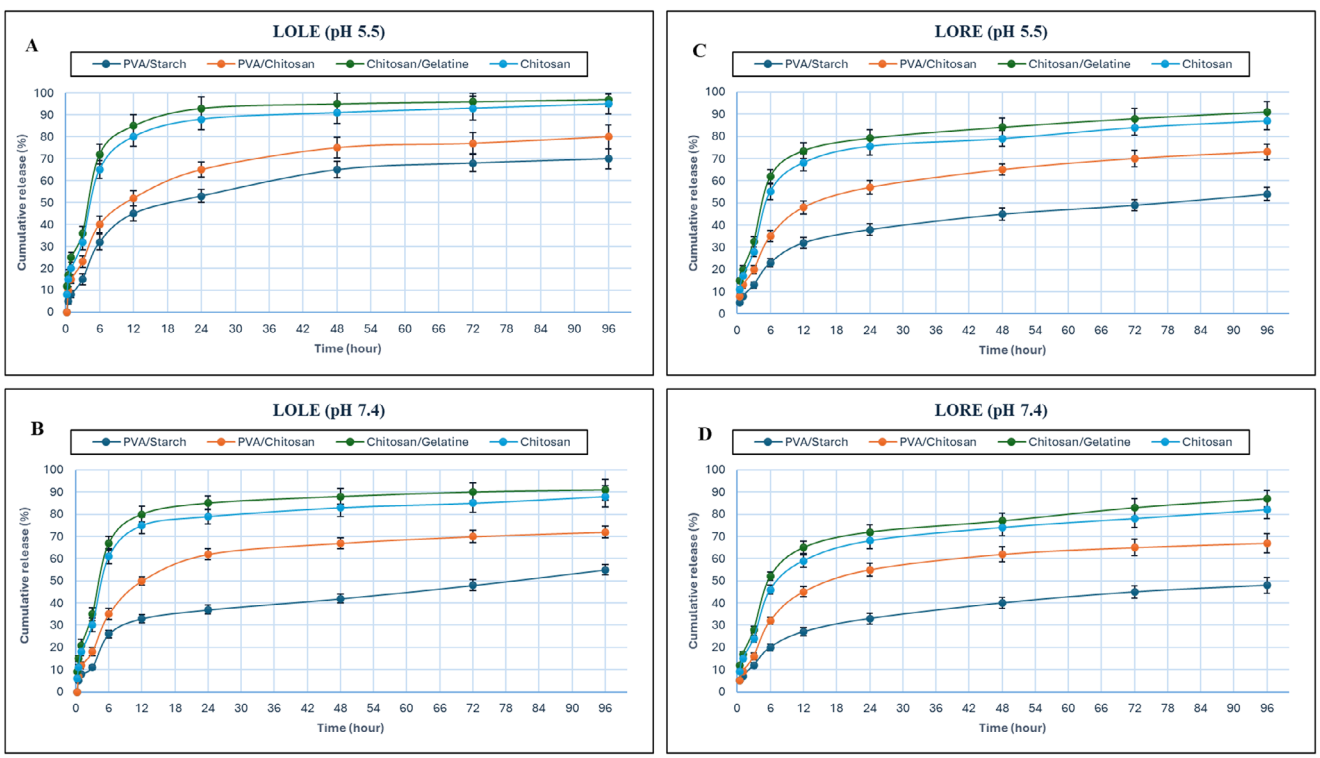


FIGURE 6 | In vitro cumulative release profiles of extract-loaded hydrogel films: (A) LOLE-loaded hydrogels at pH 5.5, (B) LOLE-loaded hydrogels at pH 7.4, (C) LORE-loaded hydrogels at pH 5.5, (D) LORE-loaded hydrogels at pH 7.4. Data are presented as mean ± SD ($n = 3$).

Among the LOLE-loaded films, chitosan/gelatin hydrogels exhibited the fastest and highest release. At pH 7.4, 67.0% of LOLE was released within 6 h and 80.0% within 12 h. Under the same conditions, cumulative release at 12 h was lower in chitosan, PVA/chitosan, and PVA/starch films, reaching 75.1%, 50.3%, and 33.5%, respectively. Under mildly acidic conditions (pH 5.5), faster release was generally observed, with 85.3% release from chitosan/gelatin and 80.2% from chitosan films at 12 h, compared with 52.0% and 45.0% from PVA/chitosan and PVA/starch films, respectively.

LORE-loaded hydrogels showed a slower release profile than LOLE-loaded hydrogels, which may be related to the more hydrophobic and resinous nature of LORE. At pH 7.4, LORE release at 12 h reached 65.0% for chitosan/gelatin, 59.3% for chitosan, 45.0% for PVA/chitosan, and 27.7% for PVA/starch films. At pH 5.5, cumulative release after 12 h increased to 73.5%, 68.2%, 48.0%, and 32.7%, respectively. In all systems, an initial rapid release phase occurred within the first 12 h, followed by a slower release phase, which can be attributed to the gradual depletion of readily diffusible extract components and the increasing contribution of diffusion through the hydrated polymeric network.

The release behavior was strongly influenced by polymer composition. Chitosan/gelatin and chitosan films generally exhibited

faster release, consistent with their higher swelling capacity and faster degradation tendency. The hydrated and more permeable structure of these matrices may facilitate faster diffusion of extract-derived compounds into the release medium. In contrast, PVA/starch films showed the slowest release, probably due to their denser and more constrained polymer network, which may limit water penetration and restrict diffusion of active compounds. PVA/chitosan films displayed an intermediate release profile, reflecting the combined contribution of PVA network stability and chitosan-associated hydration.

Statistical comparison of release percentages at corresponding time points showed that release at pH 5.5 was generally higher than at pH 7.4; however, statistically significant differences were observed only in selected formulations and time points. Therefore, the pH effect was not uniform across all systems but depended on extract type, polymer matrix, and release time. For this reason, the release behavior is described cautiously as pH-dependent within the tested pH range rather than as a broadly "smart" pH-responsive system.

To further evaluate the release mechanism, the release data were fitted to zero-order, first-order, Higuchi, and Korsmeyer–Peppas kinetic models, and the kinetic parameters are provided in Table S4. Among these models, the Korsmeyer–Peppas model provided the best fit for all formulations, with R^2 values ranging from 0.9450 to 0.9996. The release exponent (n) ranged from 0.434 to 0.669, indicating that the release mechanism varied from Fickian diffusion to anomalous transport depending on the formulation. These results suggest that extract release was governed not only by diffusion but also by matrix hydration, swelling, and polymer relaxation, consistent with the observed swelling and degradation behavior of the hydrogel films.

These results are consistent with previous studies emphasizing that controlled and sustained release of bioactive compounds is important for wound dressing materials, particularly when prolonged antioxidant or antimicrobial activity is desired. For example, Abbas et al. (2022) reported that hydrogel-based wound dressing systems can regulate the release of incorporated bioactive agents through matrix hydration, swelling, and diffusion-controlled processes [74]. Similarly, Nakipoğlu et al. (2024) observed that storax balsam-loaded polyanion–polycation hydrogels exhibited faster release under acidic conditions than under neutral or basic conditions, supporting the relevance of pH-dependent release behavior in storax-containing hydrogel systems [13]. Yao et al. (2016) also reported pH-dependent release behavior for myricetin, with faster release under acidic conditions [92]. Overall, the present findings indicate that LOLE- and LORE-loaded hydrogels exhibit matrix-dependent and pH-dependent release behavior within the tested pH range, with faster release generally observed under mildly acidic conditions.

3.15 | In Vitro Antioxidant Activity of Hydrogel Films

Excessive free radical production in the wound area can impair healing by inhibiting the migration of healthy cells. Therefore, evaluating the antioxidant activity of materials intended for wound dressings is crucial for effective recovery [93]. In this study, the antioxidant activities of hydrogel films were assessed using the DPPH radical scavenging assay at different time intervals (15 min–96 h) (Figure 7).

Among the LOLE-loaded hydrogel films, chitosan–gelatin and chitosan formulations demonstrated the highest antioxidant capacities. After 12 h, DPPH radical inhibition rates reached 67.5% and 60.3%, respectively, whereas PVA–chitosan and PVA–starch films showed lower inhibition values of 45.4% and 36.2%. In LORE-loaded hydrogel films, chitosan–gelatin and chitosan samples displayed nearly similar activities, with inhibition rates of 44.0% and 48.2% at 6 h, 57.1% and 54.3% at 12 h, and 65.2% and 58.6% at 24 h, respectively. In contrast, PVA-based films exhibited relatively lower activities, with inhibition rates of 34.1% (PVA–chitosan) and 30.3% (PVA–starch). Notably, both LOLE and LORE loaded chitosan–gelatin and chitosan hydrogels achieved more than 50% DPPH inhibition at 12 h.

These findings suggest that the hydrogel films may help reduce oxidative stress at the wound interface by providing radical-scavenging activity; however, this effect should be interpreted as an in vitro antioxidant response rather than direct evidence of accelerated wound healing. Supporting this, Demir et al. (2022) reported that increasing styrax concentration in PVA:CS cryogels enhanced both DPPH radical scavenging and metal-chelating effects, with maximum inhibition and chelation reaching 86.7% and 77.3%, respectively [12]. The higher antioxidant activity of LOLE-loaded hydrogels is consistent with the stronger radical-scavenging activity of the free leaf extract, which contained higher total phenolic and flavonoid contents than LORE. Phenolic compounds and flavonoids can contribute to DPPH radical scavenging through hydrogen atom or electron donation, and therefore their release from the hydrogel matrix is expected to directly influence the antioxidant performance of the films [57]. In addition to the extract composition, polymer matrix properties also affected the observed activity. Chitosan and chitosan/gelatin films generally showed higher antioxidant activity, which may be related to their higher swelling capacity and faster extract release. In contrast, PVA-containing films exhibited lower DPPH inhibition, probably because their denser networks restricted water uptake and delayed the diffusion of antioxidant compounds into the assay medium. Similar trends have been reported for plant extract-loaded or styrax-containing hydrogel systems, where antioxidant activity depends not only on the intrinsic radical-scavenging potential of the incorporated bioactive compounds but also on matrix hydration, swelling, and release behavior [33, 93].

3.16 | Antimicrobial Activity of Hydrogels

Determining the antimicrobial activity of materials intended for wound dressings is essential to prevent bacterial contamination arising from wound exudates. In this study, the antimicrobial activities of hydrogel films containing or lacking LOLE and LORE extracts were evaluated against *Staphylococcus aureus*, *Escherichia coli*, and *Candida albicans* at different time intervals (15 min–96 h). The amounts of hydrogels used were standardized according to the MIC values of the respective extracts (Figure 8).

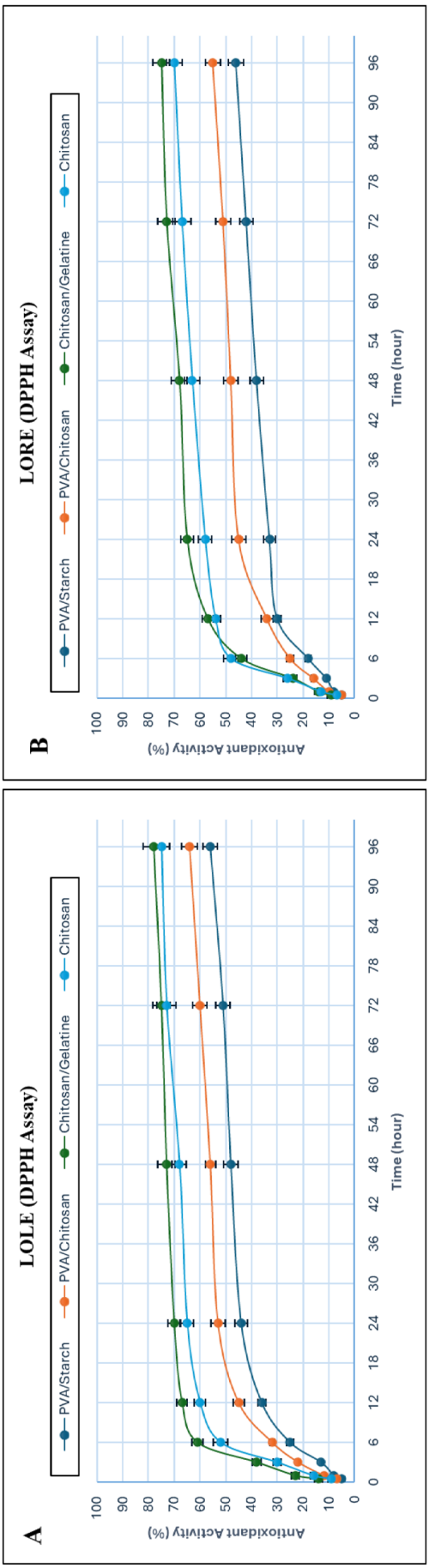


FIGURE 7 | Antioxidant activity of hydrogel films determined by the DPPH assay: (A) LOLE-loaded hydrogels and (B) LORE-loaded hydrogels. Data are presented as mean ± SD ($n = 3$).

LOLE-loaded chitosan–gelatin and chitosan films exhibited notable inhibition, showing 63.0% and 59.0% inhibition against *S. aureus*, 42.3% and 40.6% against *C. albicans*, and 31.2% and 42.2% against *E. coli* at 48 h. In contrast, PVA–chitosan and PVA–starch films displayed lower activity, with inhibition rates of 42.0% and 27.9% against *S. aureus*, 30.3% and 19.8% against *C. albicans*, and 23.6% and 17.1% against *E. coli* at the same time point.

LORE-loaded chitosan–gelatin and chitosan hydrogel films demonstrated the highest antimicrobial effects, with 69.6% and 65.3% inhibition against *S. aureus* at 24 h, 65.5% and 70.0% against *E. coli*, and 51.2% and 45.7% against *C. albicans* at 48 h. By comparison, PVA–chitosan and PVA–starch films again showed more limited antimicrobial activities, with inhibition values of 45.1% and 31.3% against *S. aureus* at 24 h, 33.4% and 25.2% against *C. albicans* at 48 h, and 40.0% and 27.5% against *E. coli* at 48 h.

Previous studies support these findings. For example, PVA:CS cryogels loaded with styrax gum were reported to have MIC values of 32 mg/L against *E. coli* and *S. aureus*, and 256 mg/L against *C. albicans* [12]. Similarly, styrax (ST)-loaded poly(ε-caprolactone) [PCL:ST (100:100)] films exhibited antimicrobial activity with MIC values of 16 mg/L against *E. coli*, *Legionella*, and *S. aureus*; 32 mg/L against *P. aeruginosa*; 64 mg/L against *E. hirae* and *C. albicans*; and 128 mg/L against *B. cereus* [23].

The stronger antimicrobial performance of LORE-loaded hydrogels can be associated with the resinous and trans-cinnamic acid-rich composition of LORE. Cinnamic acid and its derivatives have been reported to exhibit antimicrobial activity by affecting microbial membrane integrity, permeability, and intracellular metabolic processes [61]. In addition to the extract composition, the polymer matrix may also have contributed to the antimicrobial response. Chitosan-containing films generally showed stronger activity than PVA-containing systems, which may be related to the cationic nature of chitosan, its interaction with negatively charged microbial surfaces, and the higher swelling/release capacity of these matrices [94]. Conversely, the denser PVA-containing networks may have limited extract diffusion, resulting in comparatively lower antimicrobial activity.

4 | Conclusions

In this study, *Liquidambar orientalis* leaf extract (LOLE)- and resin extract (LORE)-loaded hydrogel films were successfully developed using PVA/starch, PVA/chitosan, chitosan/gelatin, and chitosan matrices. The results demonstrated that both extract type and polymer composition influenced the morphology, swelling, degradation, release behavior, and biological performance of the hydrogel films. SEM observations indicated matrix- and extract-dependent surface characteristics, while FT-IR analysis supported extract incorporation and possible intermolecular interactions within the hydrogel networks. Among the tested formulations, LOLE-loaded chitosan films showed the highest swelling capacity, reaching approximately 350%, and also exhibited the highest in vitro mass loss during the 14-day degradation study.

Release studies showed matrix-dependent and pH-dependent behavior within the tested pH range. In general, extract release

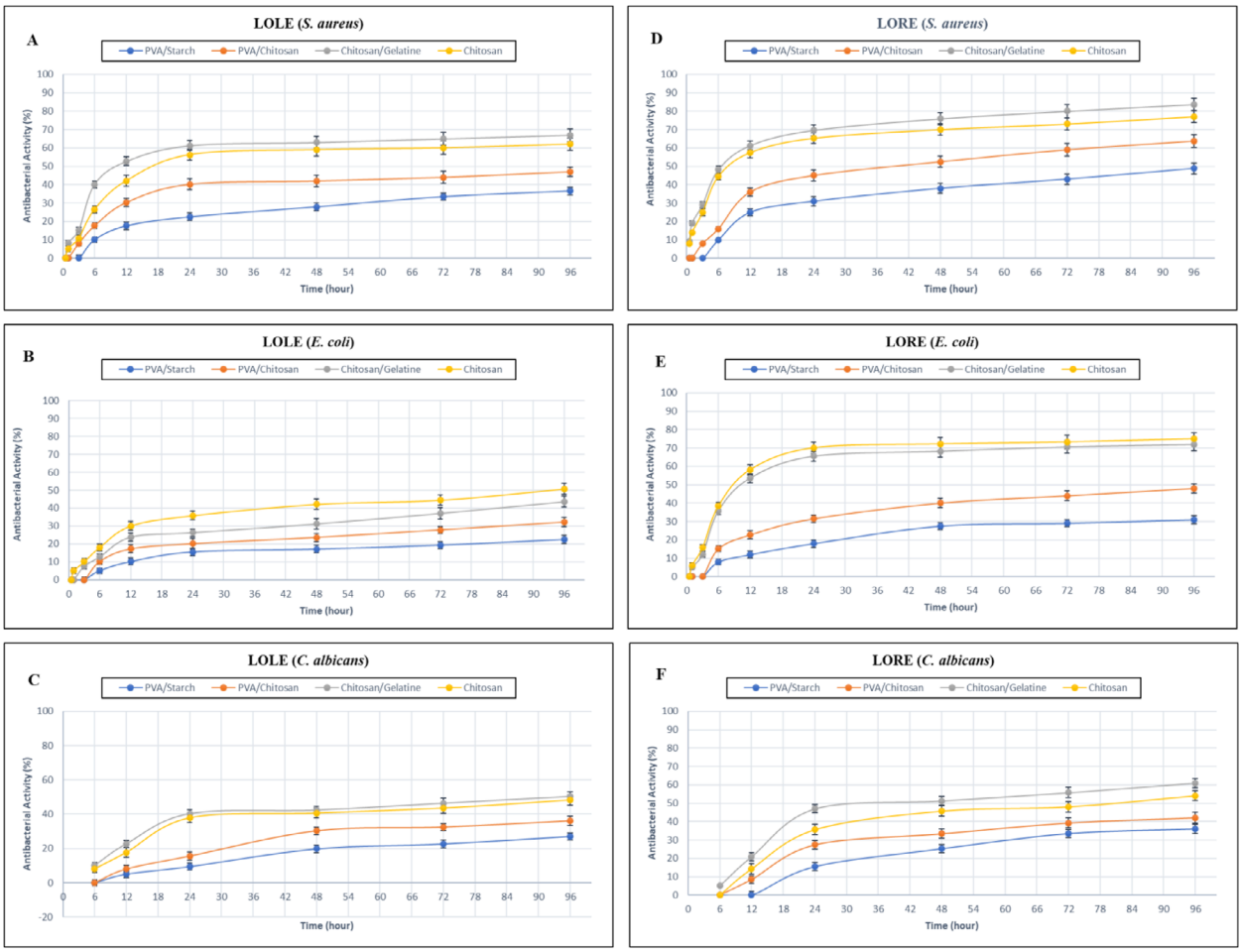


FIGURE 8 | Antimicrobial activity of hydrogel films: (A) LOLE-loaded hydrogel films against *S. aureus*, (B) LOLE-loaded hydrogel films against *E. coli*, (C) LOLE-loaded hydrogel films against *C. albicans*, (D) LORE-loaded hydrogel films against *S. aureus*, (E) LORE-loaded hydrogel films against *E. coli*, (F) LORE-loaded hydrogel films against *C. albicans*. Data are presented as mean ± SD ($n = 3$).

was faster under mildly acidic conditions (pH 5.5) than at pH 7.4, although the extent and statistical significance of this difference depended on the extract type, polymer matrix, and release time. Kinetic modeling further indicated that the Korsmeyer–Peppas model provided the best fit for all formulations, suggesting that release was governed by a combination of diffusion, matrix hydration, swelling, and polymer relaxation. These findings indicate that the developed hydrogel films can provide controlled extract release, but broader pH testing is required before defining them as fully pH-responsive systems.

The biological results showed distinct extract-dependent activity profiles. LOLE-loaded systems exhibited stronger antioxidant activity, consistent with the higher phenolic and flavonoid contents of LOLE, whereas LORE-loaded systems showed stronger antimicrobial and antibiofilm effects, probably associated with the trans-cinnamic acid-rich resin composition. The extracts also exhibited anti-quorum-sensing and enzyme-inhibitory activities. In particular, LORE showed notable tyrosinase inhibitory activity, suggesting possible relevance to pigmentation-related applications. The in vitro scratch wound closure assay showed enhanced gap closure in HEK-293T cells treated with LOLE and LORE, while the MTT assay indicated no apparent cytotoxicity under the tested conditions.

Overall, these findings support the further investigation of *L. orientalis*-derived hydrogel films as sustainable bioactive wound dressing platforms. However, several limitations should be acknowledged. First, HEK-293T cells are not skin-derived, and the scratch assay does not distinguish between cell migration and proliferation; therefore, validation using dermal fibroblasts, keratinocytes, and in vivo wound models is required. Second, the mechanical properties of the films were not evaluated, and future studies should include tensile strength, elongation at break, flexibility, and wet-state handling assessments. Finally, the chemical stability of marker compounds such as myricetin and trans-cinnamic acid during storage, release, and sterilization, as well as batch-to-batch reproducibility of extract composition, should be investigated before stronger conclusions can be drawn regarding practical wound dressing applications.

Author Contributions

Meltem Taş Küçükaydın: methodology, conceptualization, data curation, formal analysis, investigation, validation, writing – original draft. **Mehmet Emin Duru**: supervision, project administration, resources, writing – review & editing. **Aydın Demiray**: methodology, investigation. **Selçuk Küçükaydın**: data curation, formal analysis, writing – original

draft, writing – review & editing. **Özgür Ceylan**: formal analysis, methodology, resources.

Acknowledgements

The authors would like to express their gratitude for the financial support provided to this work by the Scientific and Technological Research Council of Türkiye (TUBITAK-118Z417). This study is a part of M.T.K's Ph.D. thesis. M.T.K would like to thank the TUBITAK (The Scientific and Technological Research Council of Türkiye) for the National PhD Scholarship Program (BIDEB-2211/A) and the Higher Education Commission of Türkiye (YOK) for the YOK100/2000 PhD Scholarship Program.

Conflicts of Interest

The authors declare no conflicts of interest.

Data Availability Statement

The data that support the findings of this study are available from the corresponding author upon reasonable request.

References

1. C. K. Sen, H. Wounds, and I. Burden, "Human Wounds and Its Burden: An Updated Compendium of Estimates," *Advances in Wound Care* 8 (2019): 39–48, https://doi.org/10.1089/WOUND.2019.0946/ASSET/IMAGES/LARGE/FIGURE1.JPEG.

2. J. Chanaj-Kaczmarek, M. Paczkowska, T. Osmałek, et al., "Hydrogel Delivery System Containing Calendulae flos Lyophilized Extract With Chitosan as a Supporting Strategy for Wound Healing Applications," *Pharmaceutics* 12 (2020): 634, https://doi.org/10.3390/PHARMACEUTICS12070634.

3. M. Abazari, T. Akbari, M. Hasani, et al., "Polysaccharide-Based Hydrogels Containing Herbal Extracts for Wound Healing Applications," *Carbohydrate Polymers* 294 (2022): 119808, https://doi.org/10.1016/J.CARBPOL.2022.119808.

4. M. Fathi, N. Ahmadi, A. Forouhar, and S. H. Atani, "Natural Hydrogels, the Interesting Carriers for Herbal Extracts," *Food Reviews International* 38 (2022): 713–737, https://doi.org/10.1080/87559129.2021.1885436;WGROUP:STRING:PUBLICATION.

5. S. A. El-Sherbeni and W. A. Negm, "The Wound Healing Effect of Botanicals and Pure Natural Substances Used in In Vivo Models," *Inflammopharmacology* 31 (2023): 755–772, https://doi.org/10.1007/S10787-023-01157-5.

6. Q. Jiang, Z. H. Chen, S. Bin Wang, and X. D. Chen, "Comparative Effectiveness of Different Wound Dressings for Patients With Partial-Thickness Burns: Study Protocol of a Systematic Review and a Bayesian Framework Network Meta-Analysis," *BMJ Open* 7 (2017): 013289, https://doi.org/10.1136/BMJOPEN-2016-013289.

7. S. Alven, X. Nqoro, and B. A. Aderibigbe, "Polymer-Based Materials Loaded With Curcumin for Wound Healing Applications," *Polymers* 12 (2020): 2286, https://doi.org/10.3390/POLYM12102286.

8. T. Wang, X. K. Zhu, X. T. Xue, and D. Y. Wu, "Hydrogel Sheets of Chitosan, Honey and Gelatin as Burn Wound Dressings," *Carbohydrate Polymers* 88 (2012): 75–83, https://doi.org/10.1016/J.CARBPOL.2011.11.069.

9. S. Alven, V. Khwaza, O. O. Oyedeji, and B. A. Aderibigbe, "Polymer-Based Scaffolds Loaded With Aloe Vera Extract for the Treatment of Wounds," *Pharmaceutics* 13 (2021): 961, https://doi.org/10.3390/PHARMACEUTICS13070961.

10. B. A. Khan, A. Khan, M. K. Khan, and V. A. Braga, "Preparation and Properties of High Sheared Poly(Vinyl Alcohol)/Chitosan Blended Hydrogels Films With Lawsonia Inermis Extract as Wound Dressing," *Journal of Drug Delivery Science and Technology* 61 (2021): 102227, https://doi.org/10.1016/J.JDDST.2020.102227.

11. S. Patel, S. Srivastava, M. R. Singh, and D. Singh, "Preparation and Optimization of Chitosan-Gelatin Films for Sustained Delivery of Lupeol for Wound Healing," *International Journal of Biological Macromolecules* 107 (2018): 1888–1897, https://doi.org/10.1016/J.IJBIOMAC.2017.10.056.

12. D. Demir, S. Özdemir, S. Gonca, and N. Bölgen, "Novel Styrax Liquidus Loaded Chitosan/Polyvinyl Alcohol Cryogels With Antioxidant and Antimicrobial Properties," *Journal of Applied Polymer Science* 139 (2022): 52033, https://doi.org/10.1002/APP.52033;CTYPE:STRING:JOURNAL.

13. M. Nakipoglu, Y. Özkabadayı, S. Karahan, and A. Tezcaner, "Bilayer Wound Dressing Composed of Asymmetric Polycaprolactone Membrane and Chitosan-Carrageenan Hydrogel Incorporating Storax Balsam," *International Journal of Biological Macromolecules* 254 (2024): 128020, https://doi.org/10.1016/J.IJBIOMAC.2023.128020.

14. M. E. Duru, A. Cakir, and M. Harmandar, "Composition of the Volatile Oils Isolated From The Leaves of Liquidambar Orientalis Mill. Var. Orientalis and l. Orientalis var. Integriloba From Turkey," *Flavour and Fragrance Journal* 17 (2002): 95–98, https://doi.org/10.1002/FFJ.1050;WGROUP:STRING:PUBLICATION.

15. A. Altop, G. Erener, M. E. Duru, and K. Isik, "Effects of Essential Oils From Liquidambar Orientalis Mill. Leaves on Growth Performance, Carcass and Some Organ Traits, Some Blood Metabolites and Intestinal Microbiota in Broilers," *British Poultry Science* 59 (2018): 121–127, https://doi.org/10.1080/00071668.2017.1400657.

16. T. Baytop, "Therapy With Medicinal Plants In Turkey (Past and Present)," *Publication of the Istanbul University* 312 (1999): 2–3.

17. J. M. Lingbeck, C. A. O'Bryan, E. M. Martin, J. P. Adams, and P. G. Crandall, "Sweetgum: An Ancient Source of Beneficial Compounds With Modern Benefits," *Pharmacognosy Reviews* 9 (2015): 1–11, https://doi.org/10.4103/0973-7847.156307.

18. I. Gurbuz, E. Yesilada, B. Demirci, E. Sezik, F. Demirci, and K. H. C. Baser, "Characterization of Volatiles and Anti-Ulcerogenic Effect of Turkish Sweetgum Balsam (Styrax Liquidus)," *Journal of Ethnopharmacology* 148 (2013): 332–336, https://doi.org/10.1016/J.JEP.2013.03.071.

19. G. Okmen, O. Turkcan, O. Ceylan, and G. Gork, "The Antimicrobial Activity of *Aliquidambar orientalis* mill. Against Food Pathogens and Antioxidant Capacity of Leaf Extracts," *African Journal of Traditional, Complementary and Alternative Medicines* 11 (2014): 28–33, https://doi.org/10.4314/AJTCAM.V11I5.4.

20. J. Guo, J. A. Duan, Y. Tang, and Y. Li, "Sedative and Anticonvulsant Activities of Styrax After Oral and Intranasal Administration In Mice," *Pharmaceutical Biology* 49 (2011): 1034–1038, https://doi.org/10.3109/13880209.2011.561438.

21. B. Karadeniz, Z. Ulker, and L. Alpsoy, "Genotoxic and Cytotoxic Effects of Storax In Vitro," *Toxicology and Industrial Health* 29 (2013): 181–186, https://doi.org/10.1177/0748233711428642.

22. N. Saraç and B. Şen, "Antioxidant, Mutagenic, Antimutagenic Activities, and Phenolic Compounds of Liquidambar Orientalis Mill. Var. Orientalis," *Industrial Crops and Products* 53 (2014): 60–64, https://doi.org/10.1016/J.INDCROP.2013.12.015.

23. D. Demir, S. Özdemir, S. Ceylan, M. S. Yalcin, B. Sakım, and N. Bölgen, "Electrospun Composite Nanofibers Based on Poly (ε-Caprolactone) and Styrax Liquidus (Liquidambar orientalis Miller) as a Wound Dressing: Preparation, Characterization, Biological and Cytocompatibility Results," *Journal of Polymers and the Environment* 30 (2022): 2462–2473, https://doi.org/10.1007/S10924-022-02376-7/FIGURES/3.

24. H. Y. Cakmak, H. Ege, S. Yilmaz, et al., "3D Printed Styrax Liquidus (Liquidambar Orientalis Miller)-Loaded Poly (L-Lactic Acid)/Chitosan Based Wound Dressing Material: Fabrication, Characterization, and Biocompatibility Results," *International Journal of Biological Macromolecules* 248 (2023): 125835, https://doi.org/10.1016/J.IJBIOMAC.2023.125835.

25. X. Liang, H. J. Zhong, H. Ding, et al., "Polyvinyl Alcohol (PVA)-Based Hydrogels: Recent Progress in Fabrication, Properties, and Multifunc-

tional Applications," *Polymers* 16 (2024): 2755, https://doi.org/10.3390/POLYM16192755.

26. Z. Zhao, Y. Li, Y. Xu, et al., "PLA/Starch Composites: New Applications as Control Release Materials," *Foods* 15 (2026): 454, https://doi.org/10.3390/FOODS15030454.

27. S. G. Jin, "Recent Applications of Chitosan-Based Biomaterials as Wound Dressings," *International Journal of Molecular Sciences* 27 (2026): 1637, https://doi.org/10.3390/IJMS27041637.

28. L. Maeso, P. E. Antezana, S. Municoy, et al., "Recent Advances In The Use of Gelatin as a Biomaterial for Tissue Engineering," *International Journal of Pharmaceutics* 696 (2026): 126828, https://doi.org/10.1016/J.IJPHARM.2026.126828.

29. K. Slinkard and V. L. Singleton, "Total Phenol Analysis: Automation and Comparison With Manual Methods," *American Journal of Enology and Viticulture* 28 (1977): 49–55, https://doi.org/10.5344/AJEV.1977.28.1.49.

30. Y.-K. Park, M. Koo, M. Ikegaki, and J. L. Contado, "Comparison of The Flavonoid Aglycone Contents of Apis Mellifera Propolis From Various Regions of Brazil," *Arquivos de Biologiae Technologia* 40 (1997): 97–106.

31. S. Küçükaydın, F. Çayan, G. Tel-Çayan, and M. E. Duru, "HPLC-DAD Phytochemical Profiles of Thymus Cariensis and T. Cilicicus with Antioxidant, Cytotoxic, Anticholinesterase, Anti-Urease, Anti-Tyrosinase, and Antidiabetic Activities," *South African Journal of Botany* 143 (2021): 155–163, https://doi.org/10.1016/J.SAJB.2021.07.018.

32. S. Djebili, M. Taş, A. Bouguerra, et al., "Volatile Compound Profile and Essential Oil Composition of Three Wild Algerian Aromatic Plants With Their Antioxidant and Antibiofilm Activities," *Journal of Food Measurement and Characterization* 16 (2022): 987–999, https://doi.org/10.1007/S11694-021-01220-1/TABLES/2.

33. T. Thanyacharoen, P. Chuysinuan, S. Techasakul, A. Na Lampang Noenplab, and S. Ummartyotin, "The Chemical Composition and Antioxidant and Release Properties of a Black Rice (oryza sativa l.)-Loaded Chitosan and Polyvinyl Alcohol Composite," *Journal of Molecular Liquids* 248 (2017): 1065–1070, https://doi.org/10.1016/J.MOLLIQ.2017.09.054.

34. I. Wiegand, K. Hilpert, and R. E. W. Hancock, "Agar and Broth Dilution Methods To Determine The Minimal Inhibitory Concentration (MIC) of Antimicrobial Substances," *Nature Protocols* 3 (2008): 163–175, https://doi.org/10.1038/nprot.2007.521.

35. O. Ceylan, H. Karakus, and H. Cicek, "Design and In Vitro Antibiofilm Activity of Propolis Diffusion-Controlled Biopolymers," *Biotechnology and Applied Biochemistry* 68 (2021): 789–800, https://doi.org/10.1002/BAB.1991.

36. J. H. Merritt, D. E. Kadouri, and G. A. O'Toole, "Growing and Analyzing Static Biofilms," *Current Protocols in Microbiology* 22 (2011): 1B.1.1–1B.1.18, https://doi.org/10.1002/9780471729259.MC01B01S00.

37. A. N. Tamfu, O. Ceylan, S. Kucukaydin, and M. E. Duru, "HPLC-DAD Phenolic Profiles, Antibiofilm, Anti-Quorum Sensing and Enzyme Inhibitory Potentials of Camellia sinensis (L.) O. Kuntze and Curcuma longa L," *LWT* 133 (2020): 110150, https://doi.org/10.1016/J.LWT.2020.110150.

38. T. Masuda, D. Yamashita, Y. Takeda, and S. Yonemori, "Screening for Tyrosinase Inhibitors Among Extracts of Seashore Plants and Identification of Potent Inhibitors From Garcinia Subelliptica," *Bioscience, Biotechnology, and Biochemistry* 69 (2005): 197–201, https://doi.org/10.1271/BBB.69.197.

39. C. Tyavambiza, M. Meyer, A. D. Wusu, A. M. Madiehe, and S. Meyer, "The Antioxidant and In Vitro Wound Healing Activity of Cotyledon orbiculata Aqueous Extract and the Synthesized Biogenic Silver Nanoparticles," *International Journal of Molecular Sciences* 23 (2022): 16094, https://doi.org/10.3390/IJMS232416094.

40. K. Belhouala, C. Korkmaz, M. Taş Küçükaydın, S. Küçükaydın, M. E. Duru, and B. Benarba, "Eco-Friendly Species Evernia prunastri (L.) Ach.: Phenolic Profile, Antioxidant, Anti-inflammatory, and Anticancer Properties," *ACS Omega* 9 (2024): 45719–45732, https://doi.org/10.1021/ACSOMEGA.3C10407/ASSET/IMAGES/LARGE/AO3C10407_0006.JPEG.

41. F. Altaf, M. B. K. Niazi, Z. Jahan, et al., "Synthesis and Characterization of PVA/Starch Hydrogel Membranes Incorporating Essential Oils Aimed to be Used in Wound Dressing Applications," *Journal of Polymers and the Environment* 29 (2021): 156–174, https://doi.org/10.1007/S10924-020-01866-W/FIGURES/11.

42. S. Radoor, J. Karayil, A. Jayakumar, S. Siengchin, and J. Parameswaranpillai, "A Low Cost and Eco-Friendly Membrane From Polyvinyl Alcohol, Chitosan and Honey: Synthesis, Characterization and Antibacterial Property," *Journal of Polymer Research* 28 (2021): 82, https://doi.org/10.1007/S10965-021-02415-2/METRICS.

43. O. Catanzano, G. Gomez d'Ayala, A. D'Agostino, et al., "Peg-Crosslinked-Chitosan Hydrogel Films for In Situ Delivery of Opuntia Ficus-Indica Extract," *Carbohydrate Polymers* 264 (2021): 117987, https://doi.org/10.1016/J.CARBPOL.2021.117987.

44. J. Borges-Vilches, I. Unalan, K. Fernández, and A. R. Boccaccini, "Fabrication of Biocompatible Electrospun Poly(ε-caprolactone)/Gelatin Nanofibers Loaded With Pinus radiata Bark Extracts for Wound Healing Applications," *Polymers* 14 (2022): 2331, https://doi.org/10.3390/POLYM14122331/S1.

45. C. Mohanty, M. Das, and S. K. Sahoo, "Sustained Wound Healing Activity of Curcumin Loaded Oleic Acid Based Polymeric Bandage In A Rat Model," *Molecular Pharmaceutics* 9 (2012): 2801–2811, https://doi.org/10.1021/MP300075U/ASSET/IMAGES/MEDIUM/MP-2012-00075U_0009.GIF.

46. A. Jain and S. K. Jain, "In Vitro Release Kinetics Model Fitting of Liposomes: An Insight," *Chemistry and Physics of Lipids* 201 (2016): 28–40, https://doi.org/10.1016/J.CHEMPHYSLIP.2016.10.005.

47. S. Çetinkaya, İ. Çınar Ayan, İ. Süntar, and H. G. Dursun, "The Phytochemical Profile and Biological Activity of Liquidambar orientalis Mill. var. orientalis via NF-κB and Apoptotic Pathways in Human Colorectal Cancer," *Nutrition and Cancer* 74 (2022): 1457–1473, https://doi.org/10.1080/01635581.2021.1952455;JOURNAL:JOURNAL:HNUC20;REQUESTEDJOURNAL:JOURNAL:HNUC20;WGROUP:STRING:PUBLICATION.

48. L. Gu, Z. Li, X. Zhang, M. Chen, and X. Zhang, "Identification of MAP Kinase Kinase 3 as a Protein Target of Myricetin In Non-Small Cell Lung Cancer Cells," *Biomedicine & Pharmacotherapy* 161 (2023): 114460, https://doi.org/10.1016/J.BIOPHA.2023.114460.

49. Z. Ma, G. Wang, L. Cui, and Q. Wang, "Myricetin Attenuates Depressant-Like Behavior In Mice Subjected To Repeated Restraint Stress," *International Journal of Molecular Sciences* 16 (2015): 28377–28385, https://doi.org/10.3390/IJMS161226102.

50. A. I. Elshamy, N. M. Ammar, H. A. Hassan, et al., "Topical Wound Healing Activity of Myricetin Isolated From Tecomaria capensis v. aurea," *Molecules* 25 (2020): 4870, https://doi.org/10.3390/MOLECULES25214870.

51. K. P. Prajapati, A. P. Singh, K. Dubey, et al., "Myricetin Inhibits Amyloid Fibril Formation of Globular Proteins By Stabilizing The Native Structures," *Colloids and Surfaces B: Biointerfaces* 186 (2020): 110640, https://doi.org/10.1016/J.COLSURFB.2019.110640.

52. I. Kutraite and N. Malys, "Development and Application of Whole-Cell Biosensors for the Detection of Gallic Acid," *ACS Synthetic Biology* 12 (2023): 533–543, https://doi.org/10.1021/ACSSYNBIO.2C00537/ASSET/IMAGES/LARGE/SB2C00537_0008.JPEG.

53. J. Bai, Y. Zhang, C. Tang, et al., "Gallic Acid: Pharmacological Activities and Molecular Mechanisms Involved In Inflammation-Related Diseases," *Biomedicine & Pharmacotherapy* 133 (2021): 110985, https://doi.org/10.1016/J.BIOPHA.2020.110985.

54. F. L. T. de Aquino, J. P. da Silva, J. N. de, S. Ferro, V. Lagente, and E. Barreto, "Trans-Cinnamic Acid, But Not P-Coumaric Acid Or Methyl Cinnamate, Induces Fibroblast Migration Through PKA- and p38-MAPK Signalling Pathways," *Journal of Tissue Viability* 30 (2021): 363–371, https://doi.org/10.1016/J.JTV.2021.05.003.

55. A. Cháfer, T. Fornari, R. P. Stateva, and A. Berna, "Trans-Cinnamic Acid Solubility Enhancement In The Presence of Ethanol as a Supercritical CO_2 Cosolvent," *Journal of Chemical and Engineering Data* 54 (2009): 2263–2268, https://doi.org/10.1021/JE900154X/SUPPL_FILE/JE900154X_SI_001.PDF.

56. X. Zhu, W. Yuan, Z. Li, et al., "Progress of Research on Antioxidants and Carriers for Skin Wound Repair," *Processes* 11 (2023): 2069, https://doi.org/10.3390/PR11072069.

57. J. Liu, C. Du, H. T. Beaman, and M. B. B. Monroe, "Characterization of Phenolic Acid Antimicrobial and Antioxidant Structure–Property Relationships," *Pharmaceutics* 12 (2020): 419, https://doi.org/10.3390/PHARMACEUTICS12050419.

58. M. C. Baloglu, L. Y. Ozer, B. Pirci, G. Zengin, A. Ibrahim Uba, and Y. C. Altunoglu, "Evaluation of The Potential Therapeutic Properties of Liquidambar Orientalis Oil," *Chemistry & Biodiversity* 20 (2023): 202300291, https://doi.org/10.1002/CBDV.202300291;SUBPAGE:STRING:FULL.

59. M. H. Chang, Y. P. Hsiao, C. Y. Hsu, and P. S. Lai, "Photo-Crosslinked Polymeric Matrix With Antimicrobial Functions for Excisional Wound Healing in Mice," *Nanomaterials* 8 (2018): 791, https://doi.org/10.3390/NANO8100791.

60. F. Yousefian, R. Hesari, T. Jensen, et al., "Antimicrobial Wound Dressings: A Concise Review for Clinicians," *Antibiotics* 12 (2023): 1434, https://doi.org/10.3390/ANTIBIOTICS12091434.

61. M. C. de Morais, E. de Oliveira Lima, Y. Perez-Castillo, and D. P. de Sousa, "Synthetic Cinnamides and Cinnamates: Antimicrobial Activity, Mechanism of Action, and In Silico Study," *Molecules* 28 (2023): 1918, https://doi.org/10.3390/MOLECULES28041918/S1.

62. Y. Tian, X. Jiang, J. Guo, et al., "Pharmacological Potential of Cinnamic Acid and Derivatives: A Comprehensive Review," *Pharmaceuticals* 18 (2025): 1141, https://doi.org/10.3390/PH18081141.

63. S. Avunduk and A. Kacar, "In vitro Biological Activity of Liquidambar orientalis Mill Against Pathogen and Marine Biofilm Microorganisms," *Journal of Pure and Applied Microbiology* 7 (2013): 2885–2889.

64. M. Altıparmak, M. Kule, Y. Öztürk, et al., "Skin Wound Healing Properties of Hypericum Perforatum, Liquidambar Orientalis, and Propolis Mixtures," *European Journal of Plastic Surgery* 42 (2019): 489–494, https://doi.org/10.1007/S00238-019-01538-6/FIGURES/3.

65. R. M. Slominski, T. Sarna, P. M. Płonka, C. Raman, A. A. Brożyna, and A. T. Slominski, "Melanoma, Melanin, and Melanogenesis: The Yin and Yang Relationship," *Frontiers in Oncology* 12 (2022): 842496, https://doi.org/10.3389/FONC.2022.842496/XML.

66. B. P. Kaufman, T. Aman, and A. F. Alexis, "Postinflammatory Hyperpigmentation: Epidemiology, Clinical Presentation, Pathogenesis and Treatment," *American Journal of Clinical Dermatology* 19 (2018): 489–503, https://doi.org/10.1007/S40257-017-0333-6.

67. I. Süntar, E. K. Akkol, F. S. Enol, H. Keles, and I. E. Orhan, "Investigating Wound Healing, Tyrosinase Inhibitory and Antioxidant Activities of The Ethanol Extracts of Salvia Cryptantha and Salvia Cyanescens Using In Vivo and In Vitro Experimental Models," *Journal of Ethnopharmacology* 135 (2011): 71–77, https://doi.org/10.1016/J.JEP.2011.02.022.

68. Y. H. Kong, Y. O. Jo, C. W. Cho, et al., "Inhibitory Effects of Cinnamic Acid on Melanin Biosynthesis In Skin," *Biological & Pharmaceutical Bulletin* 31 (2008): 946–948, https://doi.org/10.1248/BPB.31.946.

69. Y. Shi, Q. X. Chen, Q. Wang, K. K. Song, and L. Qiu, "Inhibitory Effects of Cinnamic Acid and Its Derivatives on The Diphenolase Activity of Mushroom () Tyrosinase," *Food Chemistry* 92 (2005): 707–712, https://doi.org/10.1016/J.FOODCHEM.2004.08.031.

70. M. Amieva and R. M. Peek, "Pathobiology of Helicobacter pylori–Induced Gastric Cancer," *Gastroenterology* 150 (2016): 64–78, https://doi.org/10.1053/J.GASTRO.2015.09.004/ASSET/890AA838-C55A-481F-9562-9459744BCCAF/MAIN.ASSETS/GR4.JPG.

71. M. Amin, F. Anwar, F. Naz, T. Mehmood, and N. Saari, "Anti-Helicobacter pylori and Urease Inhibition Activities of Some Traditional Medicinal Plants," *Molecules* 18 (2013): 2135–2149, https://doi.org/10.3390/MOLECULES18022135.

72. D. N. Iqbal, A. Ashraf, A. Nazir, S. Z. Alshawwa, M. Iqbal, and N. Ahmad, "Fabrication, Properties, and Stability of Oregano Essential Oil and Sodium Alginate-Based Wound-Healing Hydrogels," *Dose-Response* 21 (2023): 15593258231204186, https://doi.org/10.1177/15593258231204186/ASSET/E9B7179B-4D33-4A36-817F-1078C7D4B1F3/ASSETS/IMAGES/LARGE/10.1177_15593258231204186-FIG8.JPG.

73. A. Solikhin, Y. S. Hadi, M. Y. Massijaya, et al., "Properties of Poly(Vinyl Alcohol)/Chitosan Nanocomposite Films Reinforced With Oil Palm Empty Fruit Bunch Amorphous Lignocellulose Nanofibers," *Journal of Polymers and the Environment* 26 (2018): 3316–3333, https://doi.org/10.1007/S10924-018-1215-6/FIGURES/11.

74. M. Abbas, M. Arshad, M. K. Rafique, et al., "Chitosan-Polyvinyl Alcohol Membranes With Improved Antibacterial Properties Contained Calotropis Procera Extract as a Robust Wound Healing Agent," *Arabian Journal of Chemistry* 15 (2022): 103766, https://doi.org/10.1016/J.ARABJC.2022.103766.

75. B. A. Khan, S. Ullah, M. K. Khan, B. Uzair, F. Menaa, and V. A. Braga, "Fabrication, Physical Characterizations, and In Vitro, In Vivo Evaluation of Ginger Extract-Loaded Gelatin/Poly (Vinyl Alcohol) Hydrogel Films Against Burn Wound Healing In Animal Model," *Aaps Pharmscitech* 21 (2020): 323, https://doi.org/10.1208/S12249-020-01866-Y/FIGURES/8.

76. H. S. Mansur, C. M. Sadahira, A. N. Souza, and A. A. P. Mansur, "FTIR Spectroscopy Characterization of Poly (Vinyl Alcohol) Hydrogel With Different Hydrolysis Degree and Chemically Crosslinked With Glutaraldehyde," *Materials Science and Engineering: C* 28 (2008): 539–548, https://doi.org/10.1016/J.MSEC.2007.10.088.

77. Z. Cui, Z. Zheng, L. Lin, et al., "Electrospinning and Crosslinking of Polyvinyl Alcohol/Chitosan Composite Nanofiber for Transdermal Drug Delivery," *Advances in Polymer Technology* 37 (2018): 1917–1928, https://doi.org/10.1002/ADV.21850.

78. Y. F. Qian, K. H. Zhang, F. Chen, Q. F. Ke, and X. M. Mo, "Cross-Linking of Gelatin and Chitosan Complex Nanofibers for Tissue-Engineering Scaffolds," *Journal of Biomaterials Science, Polymer Edition* 22 (2011): 1099–1113, https://doi.org/10.1163/092050610x499447.

79. Y. Pranoto, S. K. Rakshit, and V. M. Salokhe, "Enhancing Antimicrobial Activity of Chitosan Films By Incorporating Garlic Oil, Potassium Sorbate and Nisin," *LWT—Food Science and Technology* 38 (2005): 859–865, https://doi.org/10.1016/J.LWT.2004.09.014.

80. B. Koc, L. Akyuz, Y. S. Cakmak, et al., "Production and Characterization of Chitosan-Fungal Extract Films," *Food Bioscience* 35 (2020): 100545, https://doi.org/10.1016/J.FBIO.2020.100545.

81. S. Ceylan, "Propolis Loaded and Genipin-Crosslinked PVA/Chitosan Membranes; Characterization Properties and Cytocompatibility/Genotoxicity Response for Wound Dressing Applications," *International Journal of Biological Macromolecules* 181 (2021): 1196–1206, https://doi.org/10.1016/J.IJBIOMAC.2021.05.069.

82. S. Li, W. Pan, M. Zhang, et al., "Chitosan-Based Dressing Materials for Burn Wound Healing," *Polymers* 17 (2025): 1647, https://doi.org/10.3390/POLYM17121647.

83. H. Wang, B. Pei, S. Yao, Y. Liu, X. Guo, and J. Tian, "Intelligent Natural Hydrogels for Wound Therapy: Spatiotemporal Microenvironment Sensing, Synergistic Regulation, and Translational Pathways," *Macromolecular Rapid Communications* 47 (2025): 00766, https://doi.org/10.1002/MARC.202500766;WGROUP:STRING:PUBLICATION.

84. P. Farnia, S. Mollaei, A. Bahrami, A. Ghassempour, A. A. Velayati, and J. Ghanavi, "Improvement of Curcumin Solubility By Polyethylene Glycol/Chitosan-Gelatin Nanoparticles (CUR-PEG/CS-G-nps)," *Biomedical Research* 27 (2016): 659–665, https://www.alliedacademies.org/articles/improvement-of-curcumin-solubility-by-polyethylene-glycolchitosangelatin-nanoparticles-curpegcsgnps.html.

85. P. A. Pawase, F. Saleem, R. Raghunathan, O. Bashir, A. M. Pathare, and S. Roy, "Recent Progress In Chitosan/Gelatin-Based Film In Food Packaging Applications: A Comprehensive Review," *International Journal of Biological Macromolecules* 339 (2026): 150000, https://doi.org/10.1016/J.IJBIOMAC.2025.150000.

86. Y. Yang, J. Fu, Q. Duan, H. Xie, X. Dong, and L. Yu, "Strategies and Methodologies for Improving Toughness of Starch Films," *Foods* 13 (2024): 4036, https://doi.org/10.3390/FOODS13244036.

87. S. Bhowmik, D. Agyei, and A. Ali, "Biodegradable Chitosan Hydrogel Film Incorporated With Polyvinyl Alcohol, Chitooligosaccharides, and Gallic Acid for Potential Application In Food Packaging," *Cellulose* 31 (2024): 8087–8103, https://doi.org/10.1007/S10570-024-06080-8.

88. P. Chuysinuan, T. Thanyacharoen, K. Thongchai, S. Techasakul, and S. Ummartyotin, "Preparation of Chitosan/Hydrolyzed Collagen/Hyaluronic Acid Based Hydrogel Composite With Caffeic Acid Addition," *International Journal of Biological Macromolecules* 162 (2020): 1937–1943, https://doi.org/10.1016/J.IJBIOMAC.2020.08.139.

89. F. Masood, M. A. Makhdoom, I. A. Channa, et al., "Development and Characterization of Chitosan and Chondroitin Sulfate Based Hydrogels Enriched With Garlic Extract for Potential Wound Healing/Skin Regeneration Applications," *Gels* 8 (2022): 676, https://doi.org/10.3390/GELS8100676.

90. J. D. Rembe, M. Witte, N. Ertas, et al., "pH Profiling Reveals Progressive Wound Acidification During Healing and Higher pH in Chronic Non-Healing Wounds: A Prospective, Multicenter Cohort Study," *Scientific Reports* 16 (2026): 10522, https://doi.org/10.1038/s41598-026-45000-7.

91. L. A. Schneider, A. Korber, S. Grabbe, and J. Dissemond, "Influence of pH on Wound-Healing: A New Perspective for Wound-Therapy?," *Archives of Dermatological Research* 298 (2007): 413–420, https://doi.org/10.1007/S00403-006-0713-X.

92. Y. Yao, M. Xia, H. Wang, et al., "Preparation and Evaluation of Chitosan-Based Nanogels/Gels for Oral Delivery of Myricetin," *European Journal of Pharmaceutical Sciences* 91 (2016): 144–153, https://doi.org/10.1016/J.EJPS.2016.06.014.

93. L. Zhang, M. Zhang, W. Tan, Z. Ma, T. Yu, and T. Zhao, "Preparation and Evaluation of Thesium Chinense Extract Loaded Polyvinyl Alcohol/Sodium Alginate Hydrogel for Wound Healing," *Polymer Bulletin* 81 (2024): 6225–6247, https://doi.org/10.1007/S00289-023-04990-4/FIGURES/13.

94. I. Aranaz, A. R. Alcántara, M. C. Civera, et al., "Chitosan: An Overview of Its Properties and Applications," *Polymers* 13 (2021): 3256, https://doi.org/10.3390/POLYM13193256.

Supporting Information

Additional supporting information can be found online in the Supporting Information section.

Supporting File: mame70265-sup-0001-SuppMat.docx.